NASA Technical Memorandum 105603

Probabilistic Evaluation of Uncertainties and Risks in Aerospace Components

A.R. Shah, M.C. Shiao, and V.K. Nagpal
Sverdrup Technology, Inc.
Lewis Research Center Group
Cleveland, Ohio

and

C.C. Chamis
National Aeronautics and Space Administration
Lewis Research Center
Cleveland, Ohio

March 1992

NASA

PROBABILISTIC EVALUATION OF UNCERTAINTIES AND RISKS IN AEROSPACE COMPONENTS

A.R. Shah, M.C. Shiao, and V.K. Nagpal
Sverdrup Technology, Inc.
Lewis Research Center Group
Brook Park, Ohio 44142

and

C.C. Chamis
National Aeronuatics and Space Administration
Lewis Research Center
Cleveland, Ohio 44135

SUMMARY

This paper summarizes a methodology developed at NASA Lewis Research Center which computationally simulates the structural, material, and load uncertainties associated with Space Shuttle Main Engine (SSME) components. The methodology has been applied to evaluate the scatter in static, buckling, dynamic, fatigue, and damage behavior of the SSME turbo pump blade. Also calculated are the probability densities of typical critical blade responses, such as effective stress, natural frequency, damage initiation, most probable damage path, etc. Risk assessments have been performed for different failure modes, and the effect of material degradation on the fatigue and damage behavior of a blade have been calculated using a multi-factor interaction equation. Failure probabilities for different fatigue cycles have been computed and the uncertainties associated with damage initiation and damage propagation due to different load cycles have been quantified. Evaluations on the effect of mistuned blades on a rotor have been made; uncertainties in the excitation frequency have been found to significantly amplify the blade responses of a mistuned rotor. The effect of the number of blades on a rotor have been studied. The autocorrelation function of displacements and the probability density function of the first passage time for deterministic and random barriers for structures subjected to random processes also have been computed. A brief discussion has been included on the future direction of probabilistic structural analysis.

I. INTRODUCTION

Evidently deterministic structural analysis methods are not sufficient to design critical structural components properly for aerospace propulsion systems like the Space Shuttle Main Engine (SSME) (ref. 1). Structural components in propulsion systems like the SSME, are subjected to a variety of complex, severe, cyclic, and transient loading conditions, including high temperature and steep temperature gradients. Most of these conditions introduce uncertainties which are quantifiable, at best, as engineering estimates. Components subjected to these complex loading conditions generally undergo nonlinear behavior which is dependent on stress, stress rate, temperature, number of load cycles, and time. Determining nonlinear behavior experimentally is difficult and perhaps impossible to describe deterministically. In addition, critical SSME structural components are relatively small and fabrication tolerances on these components can have significant effects on the component structural response. Actual responses change when components are integrated into a structural system, because actual integration generally differs by some indeterminant degree from that which was assumed when the component was designed.

Structural analyses are based on (1) loading conditions, (2) material behavior, (3) geometric configuration, and (4) supports. These four fundamental aspects are uncertain in nature (fig. 1). One direct formal way to

account for these uncertainties is to develop probabilistic structural analysis methods where all participating variables are described by appropriate probabilistic functions.

Quantifying the effects of uncertainties in loads, material behavior, geometry, support, etc. on the performance, durability, and reusability of aerospace components is complicated. At NASA Lewis Research Center Nagpal, Rubinstein, and Chamis (ref. 2) developed a methodology to study the effects of uncertainties on the geometry and material properties of a turbo pump blade. The methodology and the findings are summarized in Section V.1 of this report. This study demonstrated the advantage of being able to quantify uncertainties and the need for the probabilistic structural analysis.

NASA Lewis researchers have developed a methodology which computationally simulates uncertainties in variables occurring at the physical root level; hereinafter referred to as primitive variables; and quantify their effects on the structural response. Also, the methodology assesses the reliability and the associated risk in a given structural component. NESSUS (Numerical Evaluation of Stochastic Structures Under Stress), a general purpose finite element computer code incorporates this methodology which is generic in nature and is applicable to any structural analysis problem. A brief description of the NESSUS computer code is given in Section III.

The objective in this paper is: (1) briefly describe a methodology for computational simulation of the primitive variable uncertainties and (2) summarize the results of specific aerospace components evaluation. The specific examples used for this paper include the description of the material degradation model to predict probabilistic material behavior and its use in appropriate analyses, and a probabilistic static, dynamic, fatigue/damage analysis for a turbine blade and a mistuned bladed rotor. Section IX describes the ongoing NASA Lewis activities in the subject area and outlines some thoughts on the future direction in probabilistic structural analysis.

SYMBOLS

A = amplitude of excitation

a = crack length

B_l^{ijk} = event where node l fractures next when structure is in the damaged state D^{ijk}

C = viscous damping

C_S = covariance kernel of random process $S(t)$

C_T = covariance kernel of temperature process $T(t)$

C_f = consequential cost if failure does occur

C_i = initial cost

C_t = total cost

D^{ijk} = structure damaged at node i, j, k

D^o = structure in undamaged state

E = modulus of elasticity

F_s = cumulative distribution function for random variable s

f_s = probability density function for random variable s

K = structure stiffness

L = number of uncorrelated variables

M = mass

M_p = material property in the current state

M_{po} = material property in the reference state

N = number of cycles

n = exponent in multi-factor interaction equation model for material behavior

N_b = number of blades on the rotor

N_{MF} = number of fatigue cycles in the final state

N_{Mo} = number of fatigue cycles in the reference state

P = probability

p = exponent in multi-factor interaction equation model for material behavior

q = exponent in multi-factor interaction equation model for material behavior

S = material strength

S_c = correlation length

T = temperature

t = time

U = independent normalized random variable

Z = response variable

α = sensitivity factor

= reliability index

β = modal damping

ν = Poisson's ratio

ξ = barrier

ρ = correlation coefficient

σ = standard deviation

σ_o = effective stress

Φ = normal cumulative distribution function

ϕ = normal probability density function

ψ = phase angle

Ω = frequency of excitation

ω_i = ith natural frequency

Subscripts:

F = final condition

f = failure

i,j,k = nodes *i, j,* and *k*

o = reference condition

s = material strength

t = total

II. SSME: CRITICAL AEROSPACE COMPONENTS

The probabilistic evaluation of aerospace components at NASA Lewis is geared toward critical SSME components such as turbine blades, liquid oxygen (LOX) posts, transfer ducts, and nozzle feed lines. The SSME (fig. 2) is a reusable, high-performance, variable-thrust liquid propellant rocket engine. The SSME operates at a mixture ratio (liquid oxygen/liquid hydrogen) of 6:1 and at a chamber pressure of ~3000 psi. Sea level thrust of 375 000 lb and vacuum thrust of 470 000 lb are produced by the SSME. A throttleable thrust range of 65 to 109 percent of the rated power level provides a higher thrust level during lift-off and the initial ascent phase, and it allows an in-orbit acceleration limit of 3 g's during the final ascent phase. In a high-performance engine like the SSME, the propellants first are burned partially at a low mixture ratio under high pressure and at a relatively low temperature in the preburner; in the combustion chamber, the propellants are burned at a high mixture ratio under high pressure and at a high temperature. Such a complicated power generation process involves several engine hardware variables which have uncertainties in their mechanical, chemical, electrical, and electronic operation. Additionally, the thermo-mechanical and pressure loads also contain uncertainties. A separate computer code CLS (Composite Load Spectra) (ref. 3) simulates the effects of engine

hardware uncertainties for SSME components. Due to the load and structural uncertainties, aerospace component reliability evaluation should be based upon probabilistic methods.

III. PROBABILISTIC STRUCTURAL ANALYSIS COMPUTER CODE, NESSUS

NESSUS (refs. 4 and 5) is a comprehensive Probabilistic Finite Element Analysis computer code that can perform static, dynamic, buckling, fatigue/damage, and nonlinear analyses. Various probabilistic and finite element methods have been integrated into NESSUS in a modular fashion (fig. 3) to solve any general purpose structural analysis problem. The different modules in NESSUS can be used independently, and all the modules have been linked to automate the reliability analysis of any structure from beginning to end. Three major modules, NESSUS/PRE (preprocessor), NESSUS/FEM (finite element method), and NESSUS/FPI (fast probability integration), form the computational core of the code. The input to NESSUS, in general, involves identification of primitive variables and their statistical distributions, structural geometry, loads, boundary conditions, etc. A brief description of each NESSUS module follows:

A. NESSUS/PRE is a preprocessor which allows the user to describe any Gaussian random field over the spatial domain defined in terms of discrete finite element nodes. The Gaussian random field is defined in terms of random variables at nodes with their mean, standard deviation, and appropriate form of correlation. The NESSUS/PRE module decomposes correlated random variables into a set of uncorrelated independent vectors using modal analysis since the fast probability integration of input random variables requires them to be statistically uncorrelated and independent.

B. NESSUS/FEM is a general purpose finite element code which is used to perform structural analysis and an evaluation of sensitivity due to variation in different uncorrelated primitive variables. The response surface, defined in terms of random variables required for probabilistic analysis, in NESSUS/FPI is obtained discretely in NESSUS/FEM by perturbing independent random variables obtained from NESSUS/PRE. NESSUS/FEM incorporates an efficient perturbation algorithm to compute the sensitivity of random variables. The response sensitivity data generated is stored on a file, using a linked list database structure, for its use later.

C. NESSUS/FPI has several advanced reliability methods including fast Monte Carlo simulation. The Fast Probability Integrator being the most efficient one. The data for a given response are extracted from the database created by NESSUS/FEM in this module. The extracted numerical data is used to develop a performance model in terms of independent random variables since FPI needs explicit response functions. Using the developed performance model and statistical distribution of primitive variables, fast probability integration algorithm computes the cumulative distribution function (CDF) and sensitivity of the primitive variables for a given response.

The quantified primitive variable sensitivity and the CDF can be used to tailor the design process, to decide the types and number of tests required, to develop maintenance and inspection criteria/procedure, and to make a decision on the reusability of a component/system.

IV. PROBABILISTIC MATERIAL BEHAVIOR MODEL

Due to the variations in the manufacturing process, the microstructure of a material is never uniform. This nonuniformity means that uncertainties exist about a material's properties. (Experience has shown that material properties degrade with the type and history of loads.) Since, the loads also have uncertainties associated with them, it is important that the uncertainties in the material properties be quantified using probabilistic methods.

A generic material behavior model called the multi-factor interaction equation (MFIE) model has been developed at NASA Lewis (ref. 6). The fundamental assumption for this model is that material behavior can be simulated by primitive variables. The general form of this model is described by

$$\frac{M_p}{M_{po}} = \left[\frac{T_F - T}{T_F - T_o}\right]^n \left[\frac{S_F - \sigma}{S_F - \sigma_o}\right]^p \left[\frac{\log N_{MF} - \log N_M}{\log N_{MF} - \log N_{Mo}}\right]^q \qquad (1)$$

where subscript p denotes the material property, subscript F denotes the condition at the final stage, and subscript o denotes the condition at the reference stage. The exponents n, p, q are to be determined from the available experimental data or can be estimated from the anticipated material behavior due to a particular primitive variable. Each term in the square bracket in equation (1) is called the effect. Any number of effects can be included in the equation. In general, the generic form of the equation is:

$$\frac{M_p}{M_{po}} = \prod_{i=1}^{N} \left[\frac{V_F - V}{V_F - V_o}\right]_i^a$$

Where V denotes an effect. The exponent and each variable in the above equation can be random and have any probability distribution. The insufficiency of the experimental data can be compensated by the uncertainties in the exponent. NESSUS computer code includes the MFIE model to perform a probabilistic simulation of material behavior and subsequently evaluate the structural response.

V. PROBABILISTIC STRUCTURAL ANALYSIS OF A TURBINE BLADE

Two methods for performing a probabilistic structural analysis of a turbine blade will be discussed in this section. The first method is used to quantify primitive variable uncertainties, and it is based upon both Monte Carlo simulation, factorial design, and regression analysis concepts. The second method uses NESSUS to evaluate the reliability of a turbine blade.

V.1. Turbine Blade: Monte Carlo Simulation

The random variations in geometry and in material properties of a turbine blade have been quantified in this study. A turbo pump blade (fig. 4) is modeled with 80 triangular shell elements and 55 nodes. The probabilistic analysis for the natural frequency and the root stresses of a blade have been studied.

The methodology (ref. 2) uses Monte Carlo simulation together with factorial design and regression analysis. The simulation technique involves perturbing the geometry and material properties. The perturbation magnitudes were selected randomly and were limited to 10 percent of the original magnitude.

As an alternate to a parametric approach, a factorial design (ref. 7) was selected to perform this study. Such an approach eliminates a large number of simulation or experimental runs, and it identifies the significant and insignificant variables. The factorial design approach also provides the option of widening the magnitude range of the variables by allowing additional tests outside preselected ranges. A factorial design for three variables is illustrated in figure 5. The only limitation of the approach is that the models developed using these results are applicable only to the ranges covered in the design.

A. Response Model and Probability Distribution:

In the probabilistic simulation, models of the form

$$Y = c_o + c_1v_1 + c_2v_2 + \ldots + c_nv_n + \text{error terms} \quad (2)$$

for all the response variables are developed first; where Y is a response variable. $c_o, \ldots, c_n$, are coefficients, and $v_1, \ldots, v_n$ are the variables of the study. The coefficients and standard deviations for each of the study variables are estimated. The significance of a given variable is determined using t-tests and standard deviations. The goodness of fit and measure of randomness of the residuals are obtained using F-test and χ^2-test. A typical plot of residuals of the model is shown in figure 6. A decision is made whether to accept or reject the model based on the sparseness of the residuals. Probability distributions for the response variable were obtained by replicating simulated runs for a large number of times.

B. Results:

The variables considered for the geometry were means and standard deviations along three directions. The six variables considered for the material property were the standard deviations of the property matrix components. The magnitudes of the coefficients $c_1, c_2, \ldots$, and c_n for geometric variables and material property variables are listed in tables I and II, respectively. The coefficients related to the cross terms between geometric variables and material property variables were found to be insignificant, but they are listed in reference 2.

The results of the t-test for the coefficients in table I indicate that only the variance of perturbations along the thickness of the blade is significant because the variation in the thickness has an exponential effect on stiffness. Since the geometric perturbations along other directions are insignificant, they should be considered insignificant while the tolerances are being set. All the F-test models were good fits, but not all of them are desirable models since they include insignificant variables. Only models containing significant variables should be used.

T-test results showed (table II) that material property coefficients were statistically insignificant. This means that the scatter in material properties within 10 percent of the mean did not have significant influence on the response variables.

Probabilistic distributions of the response variables were obtained from 120 to 500 simulated replications. Figure 7 shows the probability distribution of natural frequency for the first mode of vibration, and figure 8 shows the probability distribution of root stress. The distribution estimates (1) a range of variation of a variable for given random variation in the geometric variables and (2) a probability of occurrence of a response variable. Such information would be valuable to a designer when adjusting the tolerance limits. If the range does not include any critical value, tolerances can be relaxed. This should reduce turbine blade manufacturing costs.

V.2 Turbine Blade: NESSUS Application

The SSME turbine blade (fig. 4) was analyzed probabilistically using NESSUS computer code (ref. 8). The dominant factors acting on the blade are centrifugal force, thermal load, and differential pressure across the aerofoil which are random in nature due to the uncertainties associated with them. The uncertainty in centrifugal force stems from variations in rotational speed. Uncertainty in the thermal load comes from combustion irregularities in the SSME that cause a random temperature distribution in the blade. Uncertainties in differential pressure result from pressure fluctuations.

The randomness of material properties come from nonuniformities in the composition and fabrication related variables that occur during the processing of materials prior to manufacturing. Uncertainties in the blade geometry exist as a result of the imperfections left by the manufacturing processes.

Seven random fields as listed in table III were considered in this study. All the seven random fields were assumed to be independent of each other. Mean temperature and pressure are shown in figures 9 and 10, respectively. However, the correlation coefficient between random variables at different nodes in the same field is assumed to be given by

$$\rho(X_i, X_j) = \exp(-\Delta X_{ij}/S_c) \tag{3}$$

where X_i and X_j are the ith and jth random variables in the X-coordinate random field; ΔX_{ij} is the distance between nodes i and j. S_c is the correlation length. The larger the correlation length, the greater the correlation between the random variables in a random field. When S_c is extremely large, the random field can be represented by a single random variable. When S_c approaches zero, the random variables are uncorrelated. In each correlated random field, the dependent random variables are expressed as functions of independent random variables through a decomposition procedure.

The turbine blade was modeled using 40 four-node shell elements with 55 nodes. The blade was assumed to be fixed at the root. Random variables for the coordinates and temperature were defined at each node and those for elastic modulus and lateral pressure were defined for each element.

RESULTS

The effective stresses on both the pressure and suction sides of the blade were analyzed. The mean, standard deviation, and coefficient of variation of effective stress on the pressure side are shown in figures 11(a) to (c). The largest mean effective stress is 102 ksi at the lower corner of the leading edge. The coefficient of variation associated with this critical stress was 3 percent. Using this information, a risk analysis for a particular failure mode in the blade was performed. Failure at a point occurs when the applied stress is greater than the material strength. The probability of failure was calculated by

$$P_f(i) = \int f_{\sigma_i}(X) F_{S_i}(X) dX \tag{4}$$

where f_{σ_i} is PDF of effective stress at the ith node. F_{S_i} is the CDF of strength at the ith node; this is normally distributed with the mean equal to 120 ksi and the standard deviation equal to 12 ksi.

The failure probability at each nodal point was calculated and shown in figure 11(d). As expected, the location of highest failure probability is the lower left corner (blade root, leading edge). A similar study was performed for the effective stress on the suction side as shown in figure 12. Since the stress is much lower on the suction surface than on the pressure surface, the failure probability is not as critical on the suction side.

The sensitivity of the independent random variables to the probability distribution for any response was also computed. This sensitivity information, quantified by sensitivity factors, can be used to define the role of the random variables in the reliability analysis. Sensitivity factors indicate which random variables are crucial and require more attention during the manufacturing process and more control of load and temperature conditions during operation.

The sensitivity factors for the effective stress at the airfoil leading edge root were obtained. The five most influential random variables related to thickness, elastic modulus, and rotational speed are listed in table IV. As expected, the temperature uncertainty had insignificant effect on the stress. The Z-coordinate (thickness) random field was found to be crucial. The rotational speed (which induces centrifugal forces) is another important random variable. The uncertainty of the effective stress at root will be minimized significantly if the uncertainties of the five random variables (table IV) are reduced. Such information could lead to an efficient improvement on the design and the reliability of turbine blades.

VI. PROBABILISTIC FATIGUE/DAMAGE ANALYSIS

Reliability and durability assessment are essential for component certification. Components subjected to cyclic loads ultimately develop and accumulate damage due to material property/strength degradation. A methodology for the probabilistic assessment of the life and risk associated with the components developed by Shiao and Chamis (ref. 9) is described here using the SSME turbine blade model for an example. The methodology involves a probabilistic damage analysis for the initiation of damage, the propagation of damage, and the determination of the most probable damage path.

The material property/strength degradation due to cyclic loading on the turbine blade shown in figure 13 was simulated using a multi-factor interaction equation model like the one described in Section IV of this paper. The random variables and their distributions that were used for the material behavior degradation model are described in table V. The other random variables used for structural analysis are described in table VI.

A. PROBABILISTIC DAMAGE INITIATION:

Material properties depends on the state of stress, and stress is a function of the material properties. Therefore, an iterative procedure is required to perform the probabilistic structural analysis. The following steps were followed to simulate probabilistic material properties for the model described in equation (1):

1. Predict the initial probability distributions of the material properties using reference values and the temperature field for a given fatigue life, since the stress magnitudes are unknown.
2. Compute probability distributions of stress using NESSUS.
3. Compute joint probability distribution of the stress field using:

$$P(\sigma_i \le y_i \text{ and } \sigma_j \le y_j) = \Phi(-\quad_i)\,\Phi(-\quad_j) + \int_o^{\rho_{ij}} \Phi(-\quad_i, -\quad_j, z)dz \tag{5}$$

where ρ_{ij} is defined by

$$\rho_{ij} = \sum_{k=1}^{N} \alpha_{ik}\,\alpha_{jk} \tag{6}$$

α_{ik} is the kth sensitivity factor and $\quad_i$ is the reliability index.

4. Using the distributions obtained in steps (2), (3), and MFIE (eq. (1)), obtain the probability distributions of material properties at a given fatigue cycle over the entire component.
5. repeat steps (2), (3), and (4) until the probability distributions of stresses and material properties over the entire model converge.

The damage initiation occurs when the stress is greater than the strength. The following steps can be used to obtain the risk-fatigue cycle curve:

1. For a given fatigue cycle obtain the probability distribution of effective stress, f_σ using the steps described before for probabilistic fatigue life analysis.

2. Using the probability distributions of stress, f_σ and that of strength f_s for a given fatigue cycle, calculate the probability of damage initiation p_f using

$$p_f = \int_{-\infty}^{\infty} \left(\int_{-\infty}^{x} F_s(s)ds \right) f_\sigma(x)dx \tag{7}$$

3. Repeat steps (1) and (2) to obtain risk-fatigue cycle curve for critical locations and different cycles.

Results:

The SSME blade was assumed to be subjected to a fatigue cycle which degraded its modulus, thermal expansion coefficient, and strength. The damage initiation occurs when the stress is greater than the strength. The critical points of the large displacement (points C and D) and high stress (points A and B) are shown in figure 13. As shown in figure 14, at the root of the leading edge, the probability distribution of modulus was reduced significantly after the application of cyclic loads. Material strength degradation after cyclic loads was calculated with the converged stress by the probabilistic material property model as shown in figure 15. Once the stress/strength relationships are determined at this fatigue cycle, the probability that the stress is greater than the corresponding material strength is determined from equation (7).

By varying the number of cycles and repeating the procedure described previously, a risk-fatigue cycle curve was developed for critical locations (fig. 16). This curve is useful for assessing structural risks due to fatigue. For instance, at a given acceptable risk level, the number of fatigue cycles to initial local damage can be determined. With this information available, criteria can be set for quality control, inspection intervals, and the eventual retirement of components.

B. RISK/COST ASSESSMENT

The risk-cost assessment is the evaluation of the relationship between structural reliability and the total cost of the structure. The total cost is the sum of the initial cost and cost due to consequential damage. The fraction of the cost is weighted by the probability of failure. The initial cost is the cost for component service readiness. The consequential cost is the cost incurred due to structural damage. This relationship is represented by the following equation:

$$C_t = C_i + P_f C_f \tag{8}$$

where C_t represents the total cost, C_i represents the initial cost, P_f is the probability of failure, and C_f is the consequential cost. A total cost-fatigue cycle curve was developed as shown in figure 17. Based on this curve, an inspection routine can be optimized for a given component, since the decisions on inspection intervals are generally based on the extent of the damage compared to a predetermined value of retirement-for-cause.

C. PROBABILISTIC DAMAGE ANALYSIS:

It is important to know whether a structure can still operate safely or will continue to degrade when damage has just been initiated. This can be probabilistically quantified by determining:

1. The location where damage is most likely to begin
2. The most probable damage growth path
3. The corresponding structural integrity degradation due to damage growth and loading history.

The location where damage is most likely to begin is the one where the probability of applied stress exceeding the strength is high. The probable damage path is determined as follows:

Let, D^o represents the structure in its undamaged state and D^{ijk} represents a damaged state in which damage has occurred at node *i,j,k*, consecutively. Now, let us denote the event that node *l* will damage next when the structure is in the damaged state D^{ijk}. The state indicating the collapse of the structure will be defined as the terminal state when the strain energy has sudden jump with probability of occurrence equal to 1.0. Let D^{ijk} be the terminal state. The probability of reaching the terminal state is the probability that events B_i^o, B_j^i, and B_k^{ij} all occur, which is given by

$$\text{P (damage path through nodes } i,j,k \text{ occurs)} = P\left(B_i^0 \cap B_j^i \cap B_k^{ij}\right) \tag{9}$$

where $\cap$ denotes the intersection of probability events.

There are many probable damage paths, only the two most probable are shown in figure 18 as paths 1 and 2. For path 2, the first damage location is at node 10 with a probability of damage initiation equal to 0.10. At damaged state D^{10}, the probability of the damage advancing to node 9 is equal to 0.0002. When both nodes 10 and 9 are damaged, the probability that node 14 will damage next is equal to 1.0. The change of mean strain energy is small from damage state $D^{10,9}$ to $D^{10,9,14}$. However, when the damage extends to node 18, the mean strain energy has a sudden jump. It indicates that global structural failure is imminent. Therefore, $D^{10,9,14}$ is the terminal state. Using equation (9), the probability of occurrence of path 2 is determined by

$$\text{P (path 2 occurs)} = P\left(B_{10}^0 \cap B_9^{10} \cap B_{14}^{10,9}\right) \tag{10}$$

Similarly, the probability of occurrence of path 1 is given by

$$\text{P (path 1 occurs)} = P\left(B_{15}^0 \cap B_{14}^{15} \cap B_{18}^{15,14}\right) \tag{11}$$

The probability of occurrence for path 2 is 20 times greater than that for path 1. Therefore, path 2 is the most probable damage path for that level of probability. The natural frequencies of the blade decrease when damage progresses along this path as shown in figure 19. When the damage first occurred, only the first and third modes were affected; when the damaged state is $D^{10,9,14}$, significant frequency reduction is observed.

D. RISK CONTROLLED PROBABILISTIC DAMAGE PROPAGATION

Structural components that either contain damage initially or develop damage early in their lives may still carry the service loads safely. Practical limitations in the manufacturing, inspection, and use of many structural components also prohibit complete elimination of flaws. In cases where initial flaws exist, a component's

useful lifetime is reduced significantly. Therefore, the prediction of damage propagation due to cyclic load should play an essential role in setting guidelines for inspection intervals and component retirement.

The fundamental failure mechanism for damage to propagate develops when the load effect is greater than the material resistance. Let the undamaged state be defined as the state when the probability of damage initiation is smaller than the accepted value. As load cycles increase, the material properties/strength degrades, the stress distribution changes, and the risk reaches its accepted value. At this time, a new damage mechanism is formed; the damage is either initiated or advanced, and a reliability assessment of fatigue life is needed to provide a basis to ensure a safe operation.

The probabilistic structural life of a component can be divided into two parts: initiation life and propagation life for a given risk level. The risk level is based on the cost to upgrade the material and on the cost for the consequences of structural failure. During the damage initiation life (fig. 20) the probability of damage initiation at nodal point 10 is lower than the probability for acceptable risk (when probability of failure is 10^{-03}) until the number of cycles reaches $10^{4.6}$. Damage is assumed to occur at this time. A probabilistic structural analysis was performed for this damaged structure at this fatigue cycle. The location (node 9) with the highest probability of failure was detected and the damage to the component continued.

The probability of forming a new failure mechanism is smaller than that for the acceptable risk at the beginning of the propagation life as shown in figure 21. The structure is considered to be safe and can resist additional cycles. Again, when the number of cycles increases, the material properties such as modulus, strength, damage, and toughness were degraded according to equation (1). At $10^{5.6}$ cycles, the acceptable risk level is reached and the damage advances from node 10 to node 9. The damage propagation rate is determined as

$$\frac{da}{dN} = \frac{a(9,10)}{10^{5.6}-10^{4.6}} = 1.6 \times 10^{-6} \text{ in./cycle} \qquad (12)$$

where N is the number of cycles and a(9,10) is the distance between nodes 9 and 10.

The procedure is repeated with increasing cycles until risk increases beyond acceptable levels as shown in figure 22. The structure must be retired for cause (global structure damage) after 10^5 cycles. Inspection intervals can be set during the damage propagation process to assure safety. For example, if the acceptable probability of failure is set at 10^{-3}, the structure should be inspected right after 10^5 cycles.

VII. MISTUNING OF BLADED DISKS

The inherent uncertainties in the turbine blade geometry, material properties, damping, mass, etc., result in uncertainties for dynamic characteristics. Due to these uncertainties, each blade on a rotor disk does not have the same fundamental frequency; such blades are referred to as mistuned. When the blades with even small variations in frequencies interact together on a rotor disk, their individual amplitude and dynamic stresses are altered significantly. The entire disk assembly will be affected by the vibration modes from the mistuned blades, and blade responses will be amplified significantly.

To evaluate the scatter in the amplified responses, it is important to account for the uncertainties that contribute to blade response amplifications. As described in reference 10, both structural and load uncertainties have been included in this study to quantify the amplified response uncertainties by performing a probabilistic forced dynamic response analysis by using NESSUS. The governing equation of motion for the bladed disk is

$$[M]\{\ddot{X}\} + [C]\{\dot{X}\} + [K]\{X\} = \{Ae^{i(\Omega t - \psi)}\} \quad (13)$$

where $\ddot{X}$, $\dot{X}$, and X are acceleration, velocity, and displacement, respectively. The cumulative distribution function of the blade amplitudes were obtained by using advanced first-order, second-moment analysis in NESSUS (ref. 11). The effect of the number of blades on a disk, the statistical distribution of primitive variables, and the order of excitation were evaluated (ref. 10). Representative results from reference 10, for the cases given below, are presented here to demonstrate a methodology for a probabilistic evaluation of mistuned bladed disks.

1. Disk with 10 blades
   (a) First order excitation
   (b) Second order excitation
   (c) Mean excitation frequency smaller than mean blade frequency
2. Disk with 20 blades
   (a) First order excitation
   (b) Second order excitation

Generally, rotors having more than 60 to 80 blades have significant effect of mistuning. However in this study, rotors with a small number of blades were analyzed to demonstrate a methodology.

A. MODELING CONSIDERATIONS:

Probabilistic structural analysis involves the modeling of geometry, loads, and uncertainties. The details of these modeling considerations for the bladed disk assembly analysis are described below:

Geometry - A lumped mass-spring model representing the blades and the rotor disk (fig. 23) was used for the purpose of analysis. The disk was represented by lumped masses connected by a set of radial and circumferential springs. The masses representing the blades are mounted on each lumped disk mass.

Each blade is modeled by two lumped masses, one of which corresponds to the aerofoil region and the other to the shank and fir-tree regions. The lumped masses are connected by beam elements. The radial and circumferential beam elements for the disk have only extensional stiffness representing the respective stiffness for the disk. The beam elements connecting blade masses have only bending stiffness to represent the flexural mode of vibration of the blade. Therefore, it is important to note that only the bending mode of vibration for the blade is considered in the analysis since it normally dominates the responses. Thus, the dynamic interaction between the blades comes through disk springs and masses.

Loads - The force induced on blades is due to variations in the flow around circumferential direction. The variations in the flow are considered to be periodic in nature. Therefore, the excitation would be harmonic and would be characterized by amplitude, frequency of excitation, and phase angle. The magnitude of amplitude does not matter in the case of linear analysis since the assessment is made on the responses normalized to those of a tuned rotor. The statistical distribution of the amplitude does matter, however.

In a tuned rotor, all the individual blade frequencies are the same. The frequency of excitation is selected as an integer multiple of the engine rpm. The excitation differs from blade to blade in terms of phase angle only. Since the blades are fixed around the circumference, the phase difference, ψ between two consecutive blades' excitation is given by

$$\psi = 2m\left(\frac{\pi}{N_B}\right) \tag{14}$$

where m is the integer multiple between engine rpm and frequency of excitation and N_B is the number of blades on the rotor. The modal damping used in the analysis is 3 percent (it includes material, structural, and aerodynamic).

Uncertainties:

The frequency of the blade, damping, frequency of excitation, and amplitude of excitation were considered random in this analysis. The frequency of the individual blade depends on its geometry, its material property, and its mass. Since frequency is not a primitive variable input to NESSUS, modulus of elasticity, E of blade is substituted for it as a random variable. The equivalent random variable distribution of E representing the uncertainties in mass density, geometry of blade, etc. was obtained as described in reference 10.

Normally, a rotor disk is balanced by placing blades of the same moment weight in opposite slots. To include such a physical requirement in a probabilistic model, it was assumed that the blades in opposite slots were fully correlated statistically. The mean, standard deviation, and distributions of different random variables are given in table VII.

B. RESULTS:

The cumulative probability distribution of maximum normalized amplitude of the blade on a disk is plotted in figures 24 and 25. The normalized amplitude is defined as the ratio of maximum blade response with a mistuned rotor compared to the maximum blade response with a tuned rotor. The normalized response indicates the amplification of response due to mistuning. Figure 24 shows the CDF of normalized blade amplitude for a rotor with 10 blades and figure 25 shows the CDF of normalized blade amplitude for a rotor with 20 blades.

The results show that for the same probability level for a given rotor, the amplification is higher when the excitation frequency is closer to the natural frequency of a blade. It also was observed that for a given order of excitation, the amplification increases as the number of blades increases. This is due to the fact that as the number of blades increases, a higher number of vibration modes get closer to each other.

Some additional results worth noting include (refer to table VIII):

1. When the mean excitation frequency is larger than the mean blade natural frequency, the uncertainties in the excitation frequency are more sensitive to the response CDF than those of blade frequency (figs. 26(a) and (b)).
2. When the mean excitation frequency is smaller than the mean blade natural frequency, the uncertainties of blade frequency become significantly sensitive to the response CDF as compared to those of excitation frequency (figs. 26(a) and (b)).

The sensitivity of the frequency of a blade or the frequency of excitation depends largely on the difference between the mean of each of the frequencies and their coefficient of variations. It is obvious that the uncertainty in the excitation frequency will dominate the response distribution of the rotor if:

1. The coefficient of variation for the blade frequency is small compared to that of the excitation frequency,
2. The means of the two frequencies are fairly far apart, and/or
3. The mean excitation frequency is larger than the mean blade frequency.

Uncertainties in the blade frequency and excitation forces must be considered simultaneously in order to properly assess their respective sensitivities on the response of the rotor.

VIII. PROBABILISTIC DYNAMIC ANALYSIS

Many aerospace components which require high performance, reliability and durability often operate under complex environment which include random excitations and random temperatures. These excitations and temperature variations not only degrade the material but also cause an additional randomness in the uncertain material behavior. In addition, a small variation in the structural shape may have significant effect on the structural responses. Since the excitations are time dependent, a methodology for performing probabilistic structural dynamic analysis of stochastic structures degraded by the surrounding environment has been developed by Shiao and Chamis (ref. 12). This methodology evolved from the concepts of NESSUS and consists of five parts: (1) random process decomposition, (2) a probabilistic material behavior model, (3) perturbed dynamic analysis of uncertain systems, (4) first-order, second-moment method, and (5) a set of reliability algorithms.

Random process and random field simulations are performed with a decomposition procedure. The decomposition procedure involves describing the process and field in terms of independent random variables and their respective characteristic functions; that defines the actual physical process and the associated uncertainties.

A probabilistic material behavior model defines the relationship between material properties (Young's modulus, damping ratio, thermal expansion coefficient, strength, etc.) and random phenomena (temperature, fatigue, etc.).

Perturbed dynamic analysis of uncertain systems produces perturbed time histories (dynamic responses) which are used to determine the response functions numerically in terms of independent random variables at each time.

First-order, second-moment method redefines the limit state function in the normalized probabilistic space. A set of reliability algorithms are then used to determine the important response statistics and to solve the first passage problems.

A transient analysis of a stochastic structure subjected to random excitations under severe random temperature conditions was performed using this methodology. The structure was modeled by a single degree-of-freedom oscillator (only the fundamental mode is considered in the dynamic analysis). The natural frequency of this oscillator, which is a function of the uncertain system parameters (geometry, material properties, etc.), is randomly degraded by the temperature process.

The excitations can be stationary or nonstationary evolutionary random processes. Second-order statistics of any response such as time-varying mean, standard deviation, and autocorrelation functions were determined.

The first passage problems with constant or stationary/nonstationary barriers also were evaluated. A random barrier, such as the uncertain material strength or clearance for maximum displacement, was composed of its original randomness and a variation due to the effect of random temperature and fatigue. The probability events in which crossing does or does not occur at any time are defined in terms of a reliability index and sensitivity factors from the first-order, second-moment method. The expressions for the time-varying mean crossing rate and joint mean crossing rate are described briefly later. The probability density functions of the first-passage time for various random barriers were also briefly described. The details of the methodology were explained by Shiao and Chamis (ref. 12).

(A) NUMERICAL EXAMPLES AND DISCUSSION

The methodology is applied to a single degree of freedom oscillator shown in figure 27. The initial system parameter K_o and a stationary random temperature process $T(t)$ affect the current system parameter $K(t)$ which is characterized by the following material behavior model

$$K(t) = K_o\left[\frac{T_F - T(t)}{T_F - T_o}\right]^a \tag{15}$$

where K_o, T_F, T_o are independent random variables. $T(t)$ is a stationary random process whose covariance kernel is defined by the equation

$$\text{Cov}\left[\, T(t), T(\tau)\right] = \sigma_T^2 e^{-C_T |t - \tau|} \tag{16}$$

where σ_T is the standard deviation of $T(t)$ and the constant C_T is the parameter which controls the smoothness of the random process. If $C_T = 0$, the random process reduces to a single random variable. When C_T approaches infinity, the random process becomes a white noise. The natural frequency of the oscillator is obtained by the equation

$$\omega_n(t) = \sqrt{\frac{K(t)}{M}} \tag{17}$$

where M is the lump mass. Substituting equation (15) into equation (17) yields

$$\omega_n(t) = \sqrt{\left[\frac{K_o}{M}\right]\left[\frac{T_F - T(t)}{T_F - T_o}\right]^a} \tag{18}$$

Therefore, $\omega_n(t)$ becomes a random process in time. The equation of the motion is then defined by the equation

$$\ddot{x} + 2\beta\omega_n(t)\dot{x} + \omega_n^2(t)x = F(t) \tag{19}$$

where β is the damping ratio. In the following numerical examples, these values are assumed:

M	= 300 000 lb-sec^2/in.;
$E[K_o]$	= 30 000 000 lb/in.;
$\sigma(K_o)$	= 600 lb/in.;
$E[T_F]$	= 2100 °F;
$\sigma(T_F)$	= 42 °F;
T_o	= 260 °F;
a	= 0.25;
$E[T(t)]$	= 1800 °F;
$\sigma(T(t))$	= 36 °F;
C_T	= 0.25;
β	= 0.10.

The oscillator is subjected to an evolutionary random excitation F(t) which is defined by

$$F(t) = H(t)\ S(t) \tag{20}$$

where H(t) is a deterministic function defined by

$$H(t) = \begin{cases} \dfrac{t}{t_c} & \text{when } t \le t_c \\ 1 & \text{when } t > t_c \end{cases} \tag{21}$$

and as shown in figure 28. S(t) is a stationary random process with mean E[S(t)] = S(t) = 20.0 lb and standard deviation σ_s = 2.0 lb. The covariance kernel of S(t) is defined by the equation

$$\mathrm{Cov}[S(t),\ S(\tau)] = \sigma_S^2 e^{-C_S|t\ -\ \tau|} \tag{22}$$

Again, the constant C_S will determine the smoothness of the random excitation.

A procedure is used next to decompose the random excitation S(t) and random temperature T(t) into a set of independent random variables and their respective time-varying characteristic functions. In the time interval $[-l_t,l_t]$, the process S(t) can be expanded by the equation

$$S(t) = \overline{S}(t) + \sum_{i=0}^{r} b_i f_i(t) + \sum_{j=0}^{r'} b_j f_j(t) \tag{23}$$

where b_i and b_j are the zero-mean independent random variables and

$$f_i(t) = \frac{\sqrt{2C_s\sigma_S^2}}{\omega_i^2 + C_S^2}\ \frac{\cos(\omega_i t)}{\sqrt{l_t + [\sin(2\omega_i l_t)/2\omega_i]}} \tag{24}$$

and

$$f_j(t) = \frac{\sqrt{2C_s\sigma_S^2}}{\omega_j^2 + C_S^2}\ \frac{\cos(\omega_j t)}{\sqrt{l_t + [\sin(2\omega_j l_t)/2\omega_j]}} \tag{25}$$

in which ω_i and ω_j are the solution of the transcendental equations

$$C_s - \omega_i \tan(\omega_i l_t) = 0 \tag{26}$$

and

$$\omega_j + C_s \tan(\omega_j l_t) = 0 \tag{27}$$

The random temperature process T(t) can be decomposed in a similar way.

B. RESULTS:

1. THE STATISTICS OF DYNAMIC RESPONSES

The covariance of the random excitation defined by equation (22) with C_S equal to 5, will produce a nonsmooth random process with a correlation function similar to that of earthquake records. Thirty-six independent random variables are used to represent this process. The covariance of the random temperature is defined by equation (16) with C_T equal to 0.25 because temperature oscillates slowly in time. Ten independent random variables are used to define this process. The mean, standard deviation and autocorrelation function of the dynamic displacement are determined from equations (5) to (7) of Shiao, and Chamis (ref. 12). The results are compared with Monte Carlo simulation solutions and shown in figure 29. Good agreement is observed. It also is noticed that in the time interval from 0 to 2 sec, the displacement process X(t) is nonstationary with a varying mean, standard deviation, and autocorrelation function. The process, however, becomes stationary after 2 sec.

2. THE PROBABILITY DENSITY FUNCTION OF THE FIRST-PASSAGE TIME

The first-passage problems were evaluated with different barriers and loading conditions. Two types of barriers were used and are defined by the following equations:

Type A:

$$\xi(t) = \xi_o\left(1 - \frac{t}{t_F}\right) \tag{28}$$

Type B:

$$\xi(t) = \xi_o\left(1 - \frac{t}{t_F}\right)\left[\frac{T_F - T(t)}{T_F - T_o}\right]^a \tag{29}$$

where ξ_o is the reference barrier and t_F is the final time. The degradation slope is $1/t_F$ which reflects the environmental degradation on the barriers. Type A is a deterministic barrier, whereas a Type B random barrier includes the temperature effect.

Two types of random loading were considered. The first type included C_s in equation (22) as equal to 5. This type of loading is similar to the earthquake records which are nonsmooth, random processes. The second type of loading has C_s equal to 1, which corresponds to a smooth random process. Two different degradation slopes were used, 0.02 and 0.15, to represent slow and fast environmental degradation. The mean reference barriers were chosen so that they correspond to one and three standard deviation levels of the response process. The statistics of random loads and barriers for each problem are listed in table IX. The probability density function of the first-passage time was calculated by crossing rate-based and equivalent-system based methods. The details of these methods are given by Shiao and Chamis (ref. 12). The results were compared with a Monte Carlo simulation as shown in figures 30 to 33. These results are summarized in table X.

In general, the crossing rate-based method is good for problems with a small degradation slope (0.02) subjected to nonwhite ($C_s \leq 5$) excitations for either low or high thresholds. The equivalent system based method is good for problems with a large degradation slope (0.15) subjected to nonwhite ($C_s \leq 5.0$) excitations for either low or high thresholds. When any of the following conditions are present, however, the results by the equivalent system-based method will converge to the solutions found by the Monte Carlo simulation:

1. Smoother random excitations
2. More uncertainties in the barrier
3. A larger degradation slope.

Although the method is applied to a single degree-of-freedom oscillator, it can be applied directly to a multi-degree-of-freedom system according to Shiao and Chamis (ref. 12). Generally, the computing time required by a Monte Carlo simulation is highly dependent on the degrees of freedom of the finite element model. The computing time required for the proposed methods is dependent on the number of random variables and is not sensitive to the degrees of freedom of the finite element model. Therefore, they are more attractive for complex structures or for nonlinear problems where analytical solutions do not exist. It is necessary to point out that the proposed method is not suitable for structures with high natural frequency that are subjected to white noise excitation, because an infinite number of independent random variables are required to represent this special random process; that would make the proposed method inefficient.

IX. FUTURE DIRECTION

A. Human Error Uncertainties

Many structural failures have been attributed to human factors in engineering design, analyses, maintenance, and fabrication. The human factor must be intertwined in all engineering activities to develop durable, safe, and reliable products. Most facets of the engineering process (planning, designing, manufacturing, inspection, maintenance, communication, and coordination between engineering disciplines) are limited by human errors and the degree of uncertainty associated with them. Societal, physical, professional, and psychological factors significantly influence the reliability of human performance. Therefore, human errors and their associated uncertainties in structural reliability and risk assessment should be included. An approach is being developed at NASA Lewis to simulate human performance uncertainties and include them in the structural reliability computation (ref. 13).

B. Probabilistic Creep and Viscoplastic Analysis

Inelastic behavior of many materials is a major concern for the designers and users of aerospace structures operating under severe thermal and mechanical cyclic loads and other extreme conditions. Due to the nature of the loads and the reuse of many engine components, the component material may undergo visco-elastic,

visco-plastic, and creep behavior. Characterizing material behavior during visco-elastic, visco-plastic, and creep stages is a complex problem that involves many variables and requires many experiments. The mechanics of materials under such conditions are not understood well enough for predictions to be made about the behavior of actual structures. The inelastic behavior of the material has to be simulated probabilistically and the response must be analyzed probabilistically. The probabilistic approach is the most rational way to account for the uncertainties and to predict the reliability of the component/system and the risks associated with their use.

C. Probabilistic Progressive Damage Analysis

The concepts of progressive damage analysis have already been demonstrated in Section VI. These concepts can be used and extended to develop methodologies for advanced probabilistic damage analysis on a global basis. Several damage sites can be detected, and predictions of damage growth and the effect on global response in terms of the reliability of the component and system can be estimated.

There is the possibility that several different damage sites could coalesce during their growth, and it should be necessary to make an evaluation of this compounding effect on the structure or system for life assessment. This is a major direction for research. Such studies involve the degradation of material. Therefore, the research to determine the laws governing material behavior such as the multi-factor interaction equation have to proceed in conjunction with probabilistic damage analysis research. The research also should emphasize concerns about the accuracy, efficiency, and cost effectiveness of the computation.

D. System Reliability/Risk Analysis

Each component within a structural system has several failure modes relative to the component itself and the system as a whole. Since each component performance/failure has uncertainties associated with it, the overall system performance/failure is uncertain. Different models that can integrate each component performance/failure for the evaluation of system performance and that can quantify uncertainties have to be developed. Concepts of modeling that envision system as continuous rather than by component need to be developed. Progressive damage within a component must be included in system models. Existence of multiple failure modes within the component must be accounted for in system reliability evaluations. The sensitivity of each component's performance/failure uncertainty on its system's performance/failure has to be evaluated. Models also should account for the functional (safe) and nonfunctional (fail) state of the component at any time.

A system reliability evaluation makes it easier to quantify the risk associated with a given system design or a certain performance level. Risk is looked at in these terms what event(s) can happen, what is the likelihood of that event(s) happening, and what are the consequences of the event(s). The risk can be measured in terms of human survivability, cost, comfort level, time, etc. Several models have been developed for risk analysis in terms of risk measure versus probability of occurrence.

Efforts to develop such system reliability/risk models and methodologies and to integrate them into the NESSUS computer code are already underway (ref. 14).

E. Reliability Based Certification

The certification of an aerospace component/vehicle involves the determination of its flight readiness with a predetermined level of confidence. Currently, certification procedures are based on past experience, simulation of flight in a certain number of tests, and analytical results. However, certification experience during actual mission conditions indicates in general that the procedures were not rational and reliable enough for the desired safety levels, inspection, maintenance procedures, and replacement or retirement of components.

A logical certification procedure based on a probabilistic approach that covers the entire engine performance envelop needs to be developed. Such an approach would determine the nature, type, and number of flight tests required to achieve desired safety levels in the most cost-effective manner.

The sensitivities of controlling component/engine performance variables must be quantified. Once quantified, they can be used to develop inspection schedules, inspection criteria, maintenance procedures, and component retirement schedules. Accounting for the uncertainties of primitive variables is the most rational, logical, viable and cost-effective approach for developing certification guidelines.

The developed methodologies can be used to decide certification guidelines. Probabilistic structural analysis development can produce benefits if robust certification methodologies can be developed to assure safe, reliable, and cost-justifiable missions.

F. In-Service Health Monitoring

Rocket engines health monitoring systems monitor engine parameters to detect an impending failure of the component/engine either during a developmental or an operational stage. Some critical engine parameters (beside those from films, video, and crew observations) are pressures, temperatures, rotational speeds, valve positions, loss of pump efficiency, etc. These engine parameters are normally measured through sensor data. Decisions concerning engine health are based on actual sensor data, past experience, structural analyses, etc. Reliance on sensor data alone has resulted in premature engine cutoff or unsafe engine operation.

Past experiences related to specific conditions and structural analysis itself is probabilistic in nature. To account for subtle deviations of engine parameters, reliability of sensors, multi-sensor patterns, uncertainties associated with the hardware, and the complexity of the model to predict failures from all these measured/observed/computed parameters; a probabilistic in-service health monitoring system is needed.

The probabilistic health monitoring system is not only a rational way of assessing the engine health to make critical decisions but also an aid to human operators when no authority exist to issue an engine cutoff. A successful health monitoring system will result in reduction of the developmental and operational costs and help avoid any catastrophic failures.

X. CONCLUDING REMARKS

A methodology to simulate the uncertainties of the primitive variables involved in the structural analysis/design has been described. The methodology has been incorporated into a general purpose finite element computer code, NESSUS. The uncertainties of the static, dynamic, fatigue and damage behavior of SSME turbine blade have been simulated to demonstrate the methodology. The probabilistic simulation of material behavior using the multi-factor interaction equation model has been demonstrated. The sensitivity of uncertainties in the primitive variables have been quantified in the form of sensitivity factors. The sensitivity factors are useful aids in design, inspection, maintenance procedure, and safety requirement.

The SSME turbine blade life and risk associated with its reusability have been computed. The simulation of random process has been performed in terms of basic primitive variables and their respective characteristic functions. Using this simulation procedure, a methodology for analyzing structures subjected to the stochastic process has been described, and the probability density function of the first passage time for degrading systems has been computed. Probabilistic simulation of the mistuning of rotor blades has been performed. The significance of the uncertainties associated with the forcing function in the mistuning analysis have been identified and quantified.

The methodology can be used in more complex components/systems to perform the reliability analysis, to assess life and risk, and to determine the certification procedure, number of tests required, inspection criteria, inspection intervals, and maintenance procedure. The concepts and methodology can be easily extended to simulate the role of human factor uncertainties in the structural reliability, to perform system reliability, to simulate uncertainties associated with creep and viscoplastic behavior, and to develop probability based in-service health monitoring systems.

XI. REFERENCES

1. Chamis, C.C.: Probabilistic Structural Analysis Methods for Select Space Propulsion Components. NASA TM-88861, 1986.

2. Nagpal, V.K.; Rubinstein, R.; and Chamis, C.C.: Probabilistic Structural Analysis to Quantify Uncertainties with Turbopump Blades. AIAA J., vol. 27, no. 6, June 1989, pp. 809-813.

3. Newell, J.F.; Kurth R.E.; and Ho, H.W.: Composite Load Spectra for Select Propulsion System Components. RI/RD86-123 AR-1; (Roketdyne Div., Rockwell International Corp.; NASA Contract NAS3-24382) NASA CR-179496, 1986.

4. NESSUS Users Manual. Southwest Research Institute, San Antonio, TX NASA Contract NAS3-24389, 1989.

5. Probabilistic Structural Analysis (PSAM). Annual Reports 1-6, NASA Contract NAS3-24389, 1985-1990.

6. Boyce, L.; and Chamis, C.C.: Probabilistic Constitutive Relationships for Cyclic Material Strength Models. Structures, Structural Dynamics and Materials Conference, 29th; Proceedings, Pt. 3, AIAA, 1988, pp. 1299-1306.

7. Box, G.E.P.; Hunter W.G.; and Hunter, J.S.: Statistics for Experimenters: An Introduction to Design Data Analysis, and Model Building, chs. 9, 10, 11, Wiley, New York, 1979.

8. Shiao, M.C.; Nagpal, V.K.; and Chamis, C.C.: Probabilistic Structural Analysis of Aerospace Components Using NESSUS. NASA TM-102324, 1988.

9. Shiao, M.C.; and Chamis, C.C.: A Methodology for Evaluating the Reliability and Risk of Structures Under Complex Service Environments. NASA TM-103244, 1990.

10. Shah, A.R.; Nagpal, V.K.; and Chamis, C.C.: Probabilistic Analysis of Bladed Turbine Disks and the Effect of Mistuning. NASA TM-102564, 1990.

11. Wu, Y.T.; and Burnside, O.H.: Efficient Probabilistic Structural Analysis Using an Advanced Mean value Method. Probabilistic Methods in Civil Engineering, P. D. Spanos, ed., American Society of Civil Engineers, New York, 1988, pp. 492-495.

12. Shiao, M.C.; and Chamis, C.C.: First Passage Problems: A Probabilistic Dynamic Analysis for Degrading Structures. NASA TM-103755, 1990.

13. Shah, A.R.; and Chamis, C.C.: Probabilistic Simulation of the Human Factor in Structural Reliability. Structural Integrity and Durability of Reusable Space Propulsion Systems, NASA Lewis Research Center, Cleveland, Ohio, 1991, NASA CP-10064, 1991, pp. 159-168.

14. Probabilistic Structural Analysis (PSAM). Annual Report 6, NASA Contract NAS3-24389, 1985-1990.

TABLE I. — PROBABILISTIC MODELS[a]-GEOMETRIC PERTURBATION

[Model: Dependent variable = $C_0 + C_1 \mu_1 + C_2 \mu_2 + C_3 \mu_3 + C_4 \sigma_1 + C_5 \sigma_2 + C_6 \sigma_3$ + error terms.]

Dependent variable	C_0	C_1	C_2	C_3	C_4	C_5	C_6
First frequency	6105.0	-832	-2915	-687	-8362	1897	-9348
Second frequency	9475.1	-1374	-2961	-408	-11398	-3869	-9095
Third frequency	15792.0	-9434	27592	-7944	-17663	-4899	-44147
Root stress	63323.0	49707	103320	4177	88960	-48191	283960
Tip displacement[b]	1.96	11.9	128.7	20.6	-13.2	-41.9	6.7

[a]F tests indicated that all models are good fits.
[b]Tip displacement coefficients to be divided by 1000.

TABLE II. — PROBABILISTIC MODELS[a]-MATERIAL PROPERTIES PERTURBATION

[Model: Dependent variable = $C_0 + C_1 E_{11} + C_2 E_{12} + C_3 E_{13} + C_4 E_{22} + C_5 E_{23} + C_6 E_{33}$ + error terms.]

Dependent variable	C_0	C_1	C_2	C_3	C_4	C_5	C_6
First frequency	4769.7	-239.1	-64.1	-55.1	-69.0	63.2	47.1
Second frequency	5501.9	-342.6	-25.5	-96.7	-250.7	110.4	52.2
Third frequency	9653.0	-788.6	-0.8	-61.5	-909.6	185.4	-63.6
Root stress	97673.0	498.0	-4001.0	-1336.0	-9962.0	-12154.0	16701
Tip displacement[b]	12.1	3.1	0.4	0.1	1.1	0.5	1.33

[a]F tests indicated that all models are not good fits.
[b]Tip displacement coefficients to be divided by 1000.

TABLE III. — PRIMITIVE VARIABLE DISTRIBUTION PROBABILISTIC STRUCTURAL ANALYSIS OF TURBINE BLADE

Random fields	Number of dependent random variables	Mean	Standard deviation/ Cov	Correlation length, in.	Number of independent random variables
X-coordinate	55	Deterministic coordinate	0.01 in.	5.0	13
Y-coordinate	55	Deterministic coordinate	0.01 in.	5.0	13
Z-coordinate	55	Deterministic coordinate	0.01 in.	5.0	13
Temperature	55	Steady state temperature	60 °F	3.0	22
Modulus	40	23×10^6 psi	0.10 (Cov)	3.0	16
Pressure	36	Steady state pressure	0.20 (Cov)	0.0	36
Rotational speed	1	40 000 rpm	0.01 (Cov)	---	1

TABLE IV. — FIVE MOST INFLUENTIAL INDEPENDENT RANDOM VARIABLES TO THE EFFECTIVE STRESS AT ROOT

Random fields	*n*th Independent random variable in each field	Sensitivity factor	Ranking
Z-coordinate	1	0.204	4
Z-coordinate	2	0.610	1
Z-coordinate	5	0.273	3
Elastic modulus	12	0.188	5
Rotational speed	1	0.326	2

TABLE V. — RANDOM VARIABLE PROBABILITY DISTRIBUTIONS FOR PROBABILISTIC MATERIAL PROPERTY MODEL

Variable	Distribution type	Mean	Standard deviation
T_F, °F	Normal	2750	51.4
T_o, °F	Normal	68	2.04
S_F, ksi	Normal	212.0	10.6
σ_o	Constant	.0	.0
N_{MF}	Lognormal	10^8	5×10^7
N_{Mo}	Lognormal	10^3	50
n_E	Normal	0.25	0.0075
p_E	Normal	0.25	0.0075
q_E	Normal	0.25	0.0075
n_v	Normal	-0.25	0.0075
p_v	Normal	0.25	0.0075
q_v	Normal	0.25	0.0075
n_S	Normal	0.25	0.0075
p_S	Normal	0.25	0.0075
q_s	Normal	0.25	0.0075

TABLE VI. — RANDOM VARIABLE INPUT DATA FOR TURBINE BLADE

Random fields	Number of dependent random variables	Mean	Standard deviation (or coefficient of variation)	Correlation length
X coordinate	55	Determinstic coordinate	0.01 in.	5.0
Y coordinate	55	Deterministic coordinate	0.01 in.	5.0
Z coordinate	55	Deterministic coordinate	0.01 in.	5.0
Temperature	55	Steady-state temperature	60 °F	3.0
Elastic modulus	40	23 000 000 psi	0.10 (coefficient of variation)	3.0
Pressure	36	Steady-state pressure	0.20 (coefficient of variation)	0.0
Rotational speed	1	40 000 rpm	0.01 (coefficient of variation)	N/A
Poisson's ratio	40	0.45×10^{-5} in./°F	0.45×10^{-6} in./°F	3.0

TABLE VII. — RANDOM VARIABLES USED FOR PROBABILISTIC ASSESSMENT OF A MISTUNED ROTOR

(a) Disk with 10 blades.

Primitive variable	Mean	Coefficient of variation, %
Frequency of blade (cps)	959.0	1.0
Damping	3 percent	5.0
(a) Second-order excitation		
Frequency (cps)	1909.86	5.0
Amplitude	100.0	5.0
(b) Third-order excitation		
Frequency (cps)	2864.8	5.0
Amplitude	100.0	5.0
(c) Mean excitation frequency smaller than mean blade frequency		
Frequency (cps)	477.5	5.0
Amplitude	100.0	5.0

(b) Disk with 20 blades.

Primitive variable	Mean	Coefficient of variation, %
Frequency of Blade (cps)	959.0	1.0
Damping	3 percent	5.0
(a) Second-order excitation		5.0
Frequency (cps)	1909.86	5.0
Amplitude	100.0	
(b) Third-order excitation		5.0
Frequency (cps)	2864.8	5.0
Amplitude	100.0	

Note: Statistical distribution of all random variables considered normal.

TABLE VIII. — SENSITIVITY FACTORS

[Case (a), (b), (c), etc. refer to those of table VII.]

(a) Disk with 10 blades.

Probability	Primitive variable	Sensitivity
(a) 0.99999	Blade frequency Excitation frequency	0.15 .916
(b) 0.99999	Blade frequency Excitation frequency	0.017 .953
(c) 0.99999	Blade frequency Excitation frequency	0.527 .627

(b) Disk with 20 blades.

Probability	Primitive variable	Sensitivity
(a) 0.99999	Blade frequency Excitation frequency	0.124 .915
(b) 0.99999	Blade frequency Excitation frequency	0.051 .91

TABLE IX. — STATISTICS FOR RANDOM LOADS AND BARRIERS

Figure number	Random barriers				Loads
	Barrier type	Reference barrier		Degradation slope	Cs in equation (22)
		Mean	Cov		
30a	A	0.37	0.00	0.02	5
30b	A	0.47	0.00	0.02	5
30c	A	0.37	0.00	0.15	5
30d	A	0.47	0.00	0.15	5
31a	A	0.37	0.00	0.02	1
31b	A	0.47	0.00	0.02	1
31c	A	0.37	0.00	0.15	1
31d	A	0.47	0.00	0.15	1
32a	B	0.58	0.10	0.02	5
32b	B	0.74	0.10	0.02	5
32c	B	0.58	0.10	0.15	5
32d	B	0.74	0.10	0.15	5
33a	B	0.58	0.10	0.02	1
33b	B	0.74	0.10	0.02	1
33c	B	0.58	0.10	0.15	1
33d	B	0.74	0.10	0.15	1

TABLE X. — SUMMARY OF RESULTS FOR FIRST PASSAGE PROBLEMS

Case	Barrier type	Random excitation S(t)	Barrier degradation slope	Remarks
1	Type A deterministic	$C_s = 5.0$	0.02	CRB[a] method performs well Figure 30(a) Figure 30(b)
2	Type A deterministic	$C_s = 5.0$	0.15	ESB[b] method performs well Figure 30(c) Figure 30(d)
3	Type A deterministic	$C_s = 1.0$	0.02	ESB method shows improvement over Case (1) Figure 31(a) Figure 31(b)
4	Type A deterministic	$C_s = 1.0$	0.15	CRB method shows improvement over Case (2) Figure 31(c) Figure 31(d)
5	Type B random	$C_s = 5.0$	0.02	CRB method performs well and ESB method is satisfactory Figure 32(a) Figure 32(b)
6	Type B random	$C_s = 5.0$	0.15	ESB method performs well Figure 32(c) Figure 32(d)
7	Type B random	$C_s = 1.0$	0.02	Both methods performs well Figure 33(a) Figure 33(b)
8	Type B random	$C_s = 1.0$	0.15	Both methods performs well Figure 33(c) Figure 33(d)

[a] Crossing rate based.
[b] Equivalent system based.

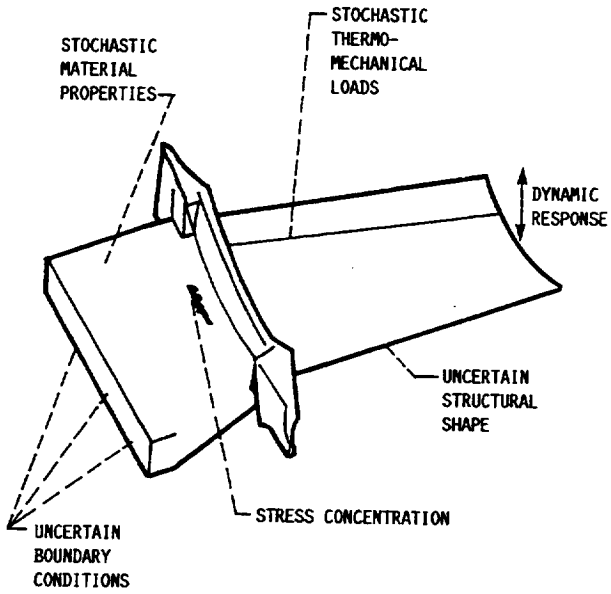

FIGURE 1. - PROBABILISTIC STRUCTURAL ANALYSIS PROBLEM.

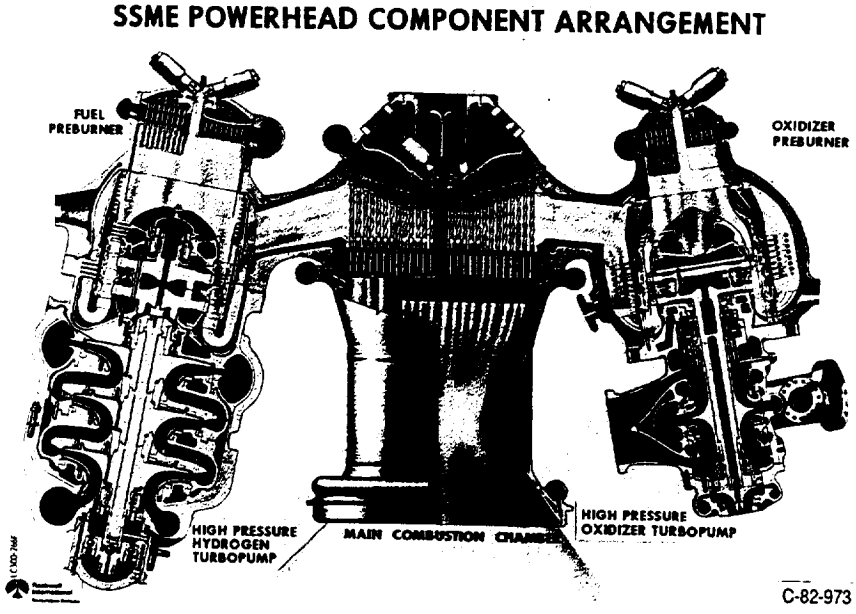

FIGURE 2.—SPACE SHUTTLE MAIN ENGINE.

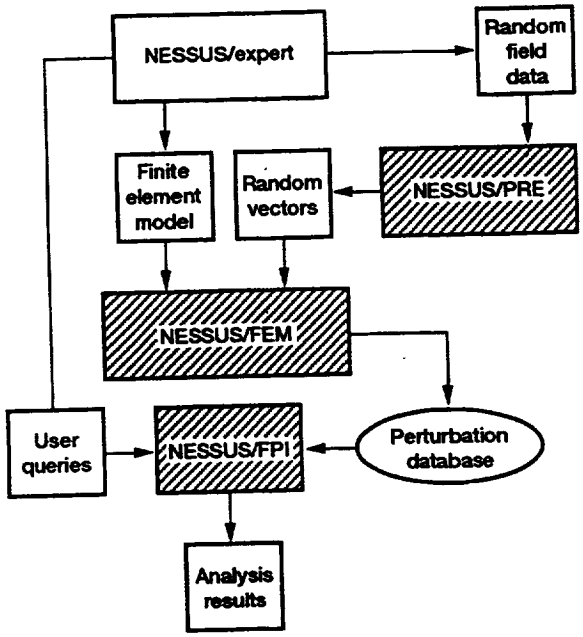

FIGURE 3.—NESSUS, COMPUTER CODE MODULES.

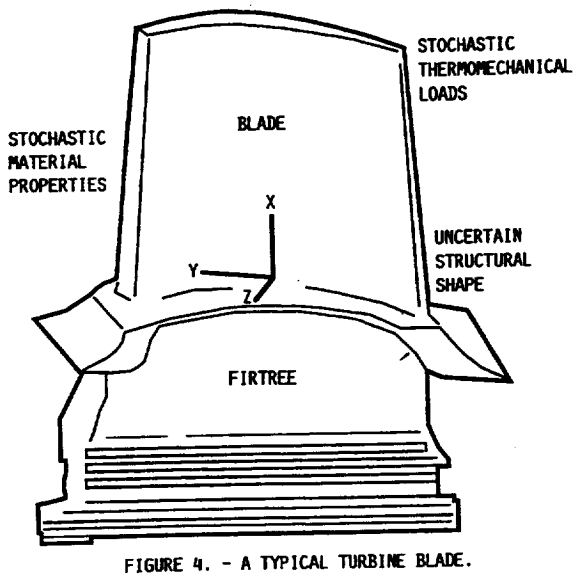

FIGURE 4. - A TYPICAL TURBINE BLADE.

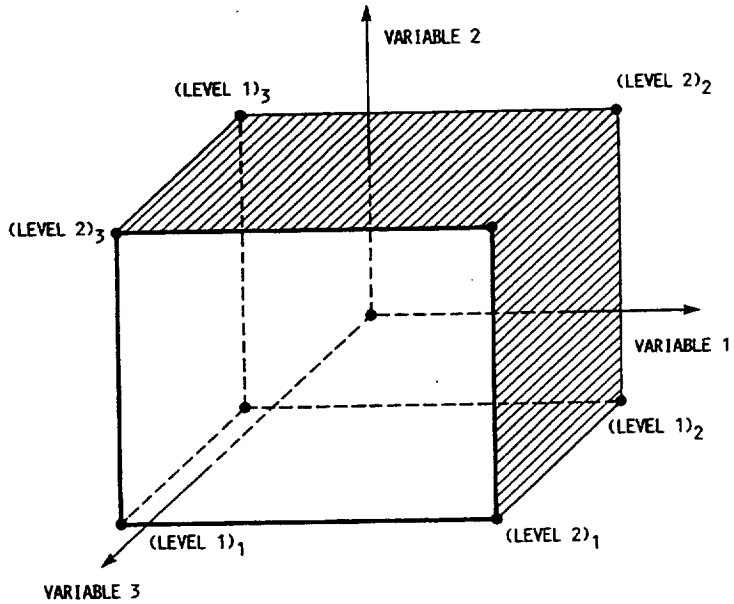

FIGURE 5.- FACTORIAL DESIGN FOR THREE VARIABLES.

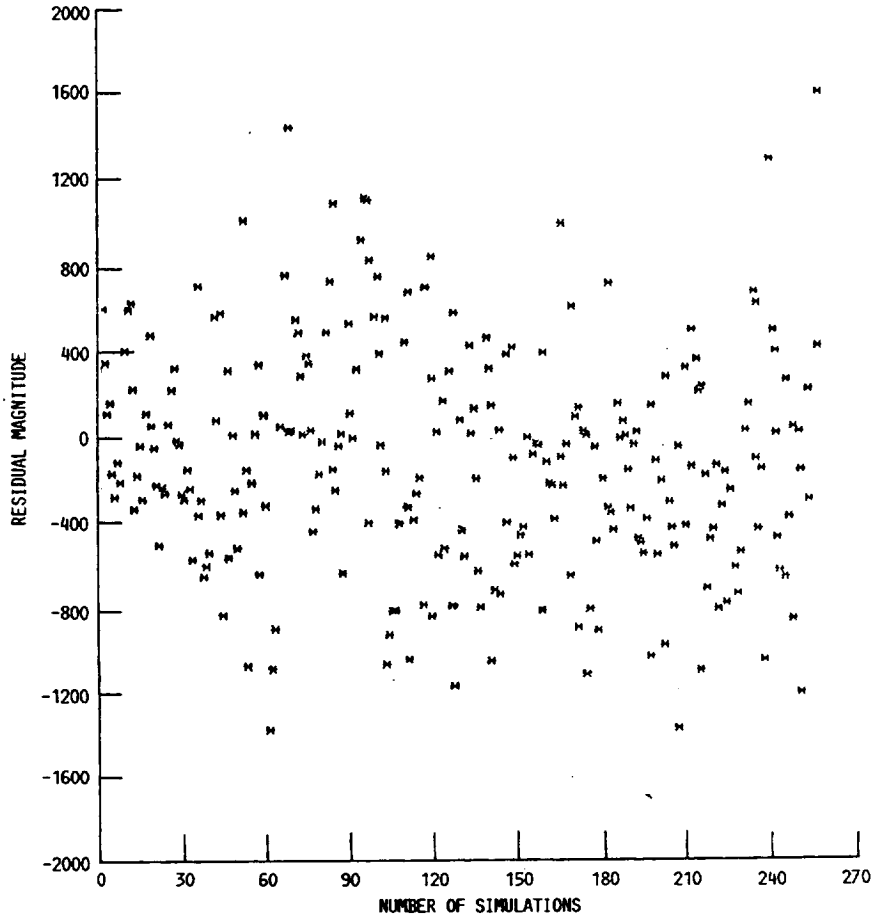

FIGURE 6. - DISTRIBUTION OF RESIDUALS.

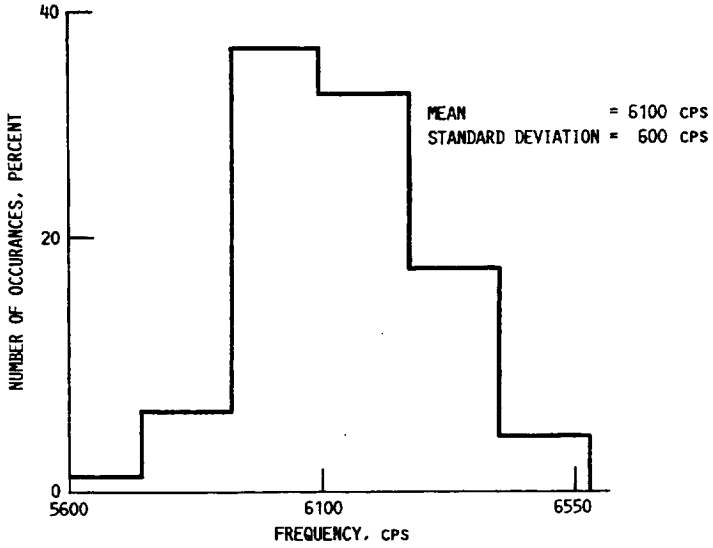

FIGURE 7. - PROBABILITY DISTRIBUTION OF FIRST NATURAL FREQUENCY.

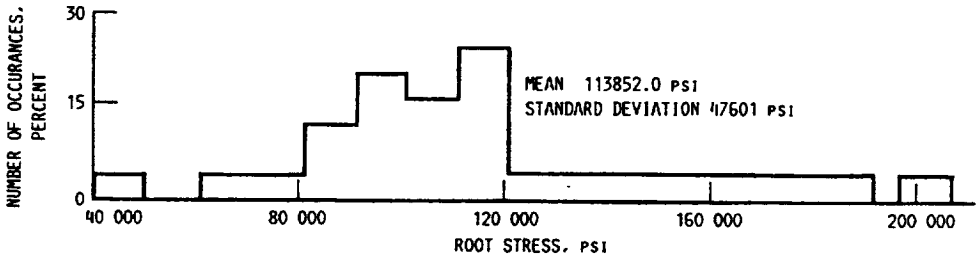

FIGURE 8. - PROBABILITY DISTRIBUTION OF ROOT STRESS.

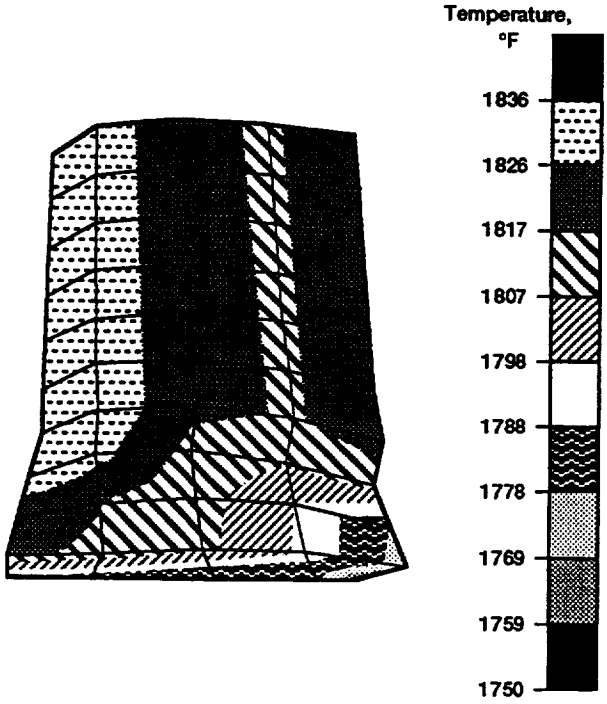

FIGURE 9.—STEADY STATE TEMPERATURE DISTRIBUTION.

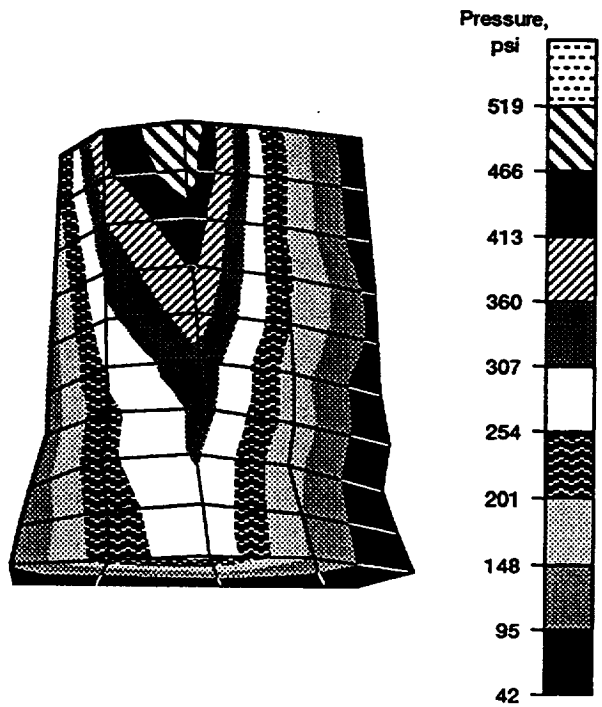

FIGURE 10.—STEADY STATE PRESSURE DISTRIBUTION.

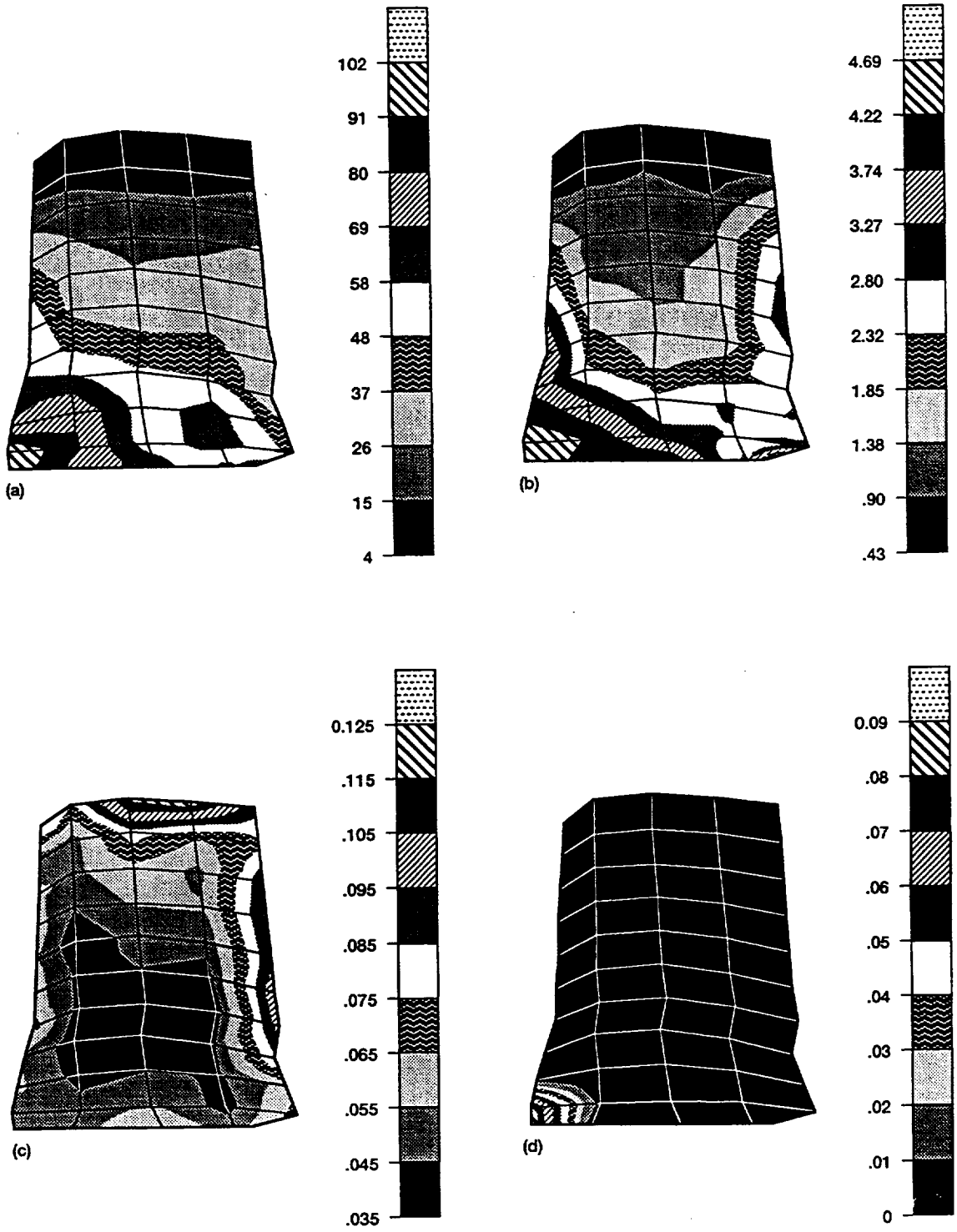

(a) Mean (pounds per square inch).
(c) Coefficient of variation.

(b) Standard deviation (pounds per square inch).
(d) Probability of failure.

FIGURE 11.—EFFECTIVE STRESS ON PRESSURE SIDE.

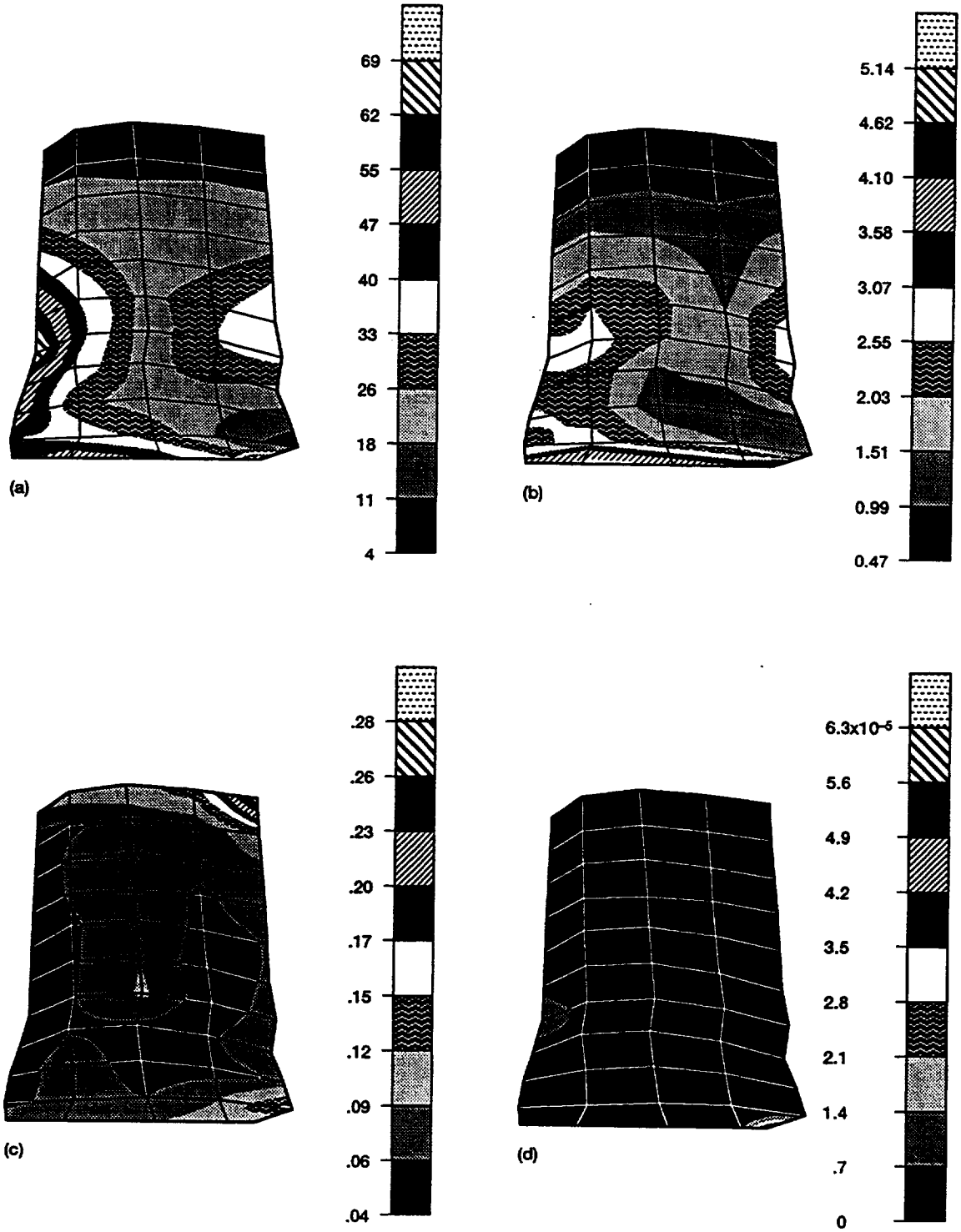

(a) Mean (pounds per square inch).
(c) Coefficient of variation.

(b) Standard deviation (pounds per square inch).
(d) Probability of failure.

FIGURE 12.—EFFECTIVE STRESS ON SUCTION SIDE.

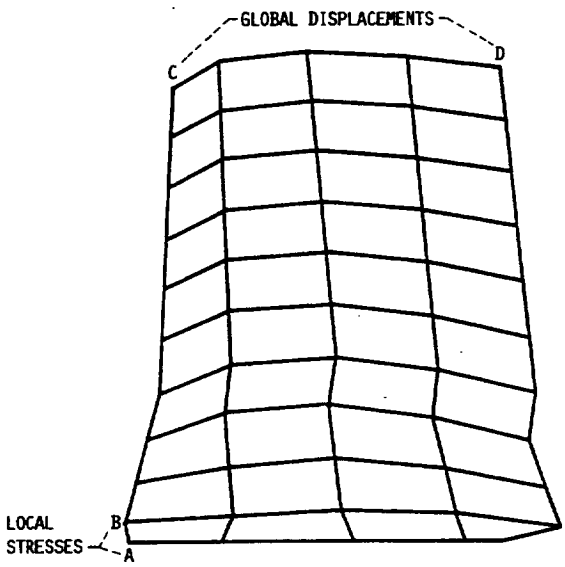

FIGURE 13. - SPACE SHUTTLE MAIN ENGINE (SSME) BLADE SHOWING LOCATIONS WHERE PROBABILISTIC STRUCTURAL RESPONSE WAS EVALUATED.

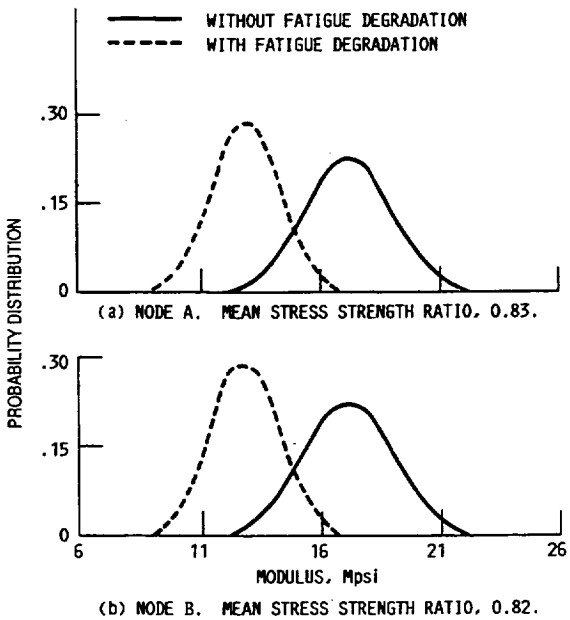

(b) NODE B. MEAN STRESS STRENGTH RATIO, 0.82.

FIGURE 14. - PROBABILISTIC ELASTICITY MODULUS SIMULATED BY USING THE GENERIC PROBABILISTIC MATERIAL PROPERTY MODEL. (NODES A AND B SHOWN IN FIG. 13).

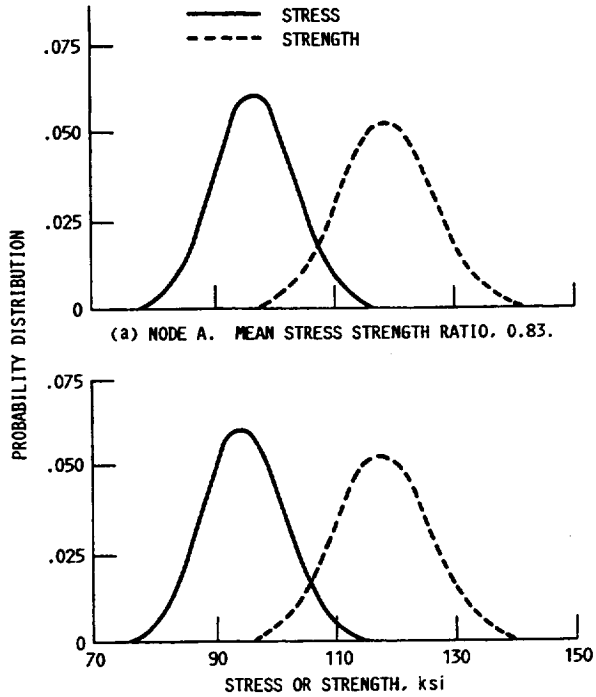

(b) NODE B. MEAN STRESS STRENGTH RATIO, 0.82.

FIGURE 15. - PROBABILISTIC FATIGUE STRESS OR STRENGTH SIMULATED BY USING THE GENERIC PROBABILISTIC MATERIAL PROPERTY MODEL. (NODES A AND B SHOWN IN FIG. 13).

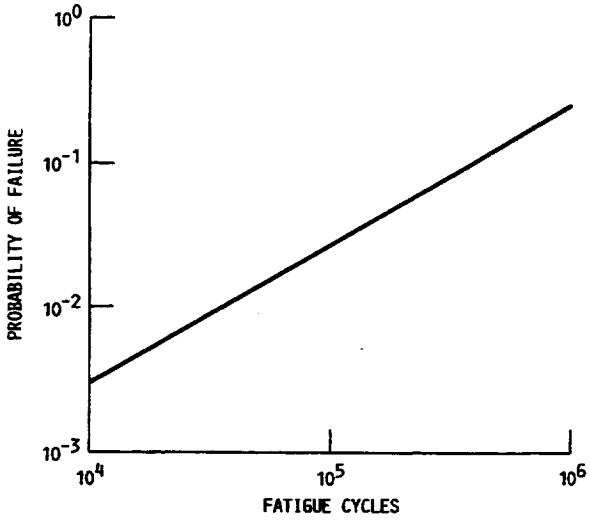

FIGURE 16. - PROBABILITY OF LOCAL FAILURE AT NODE A (FIG. 13) DUE TO FATIGUE CYCLES.

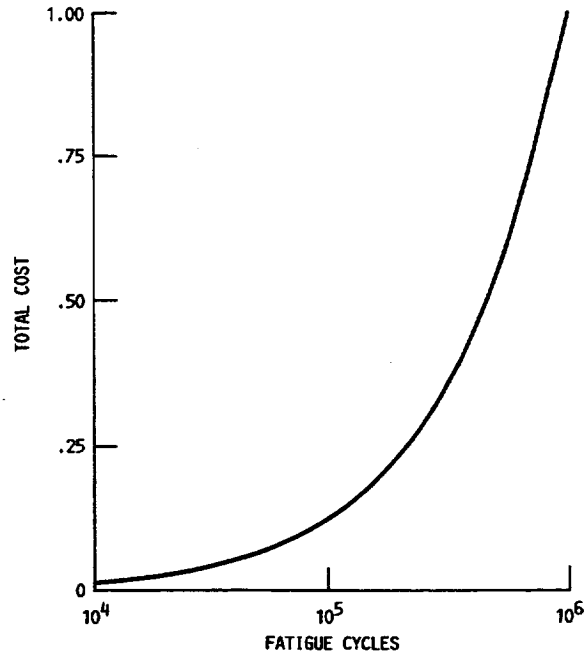

FIGURE 17. - RISK-COST ASSESSMENT.

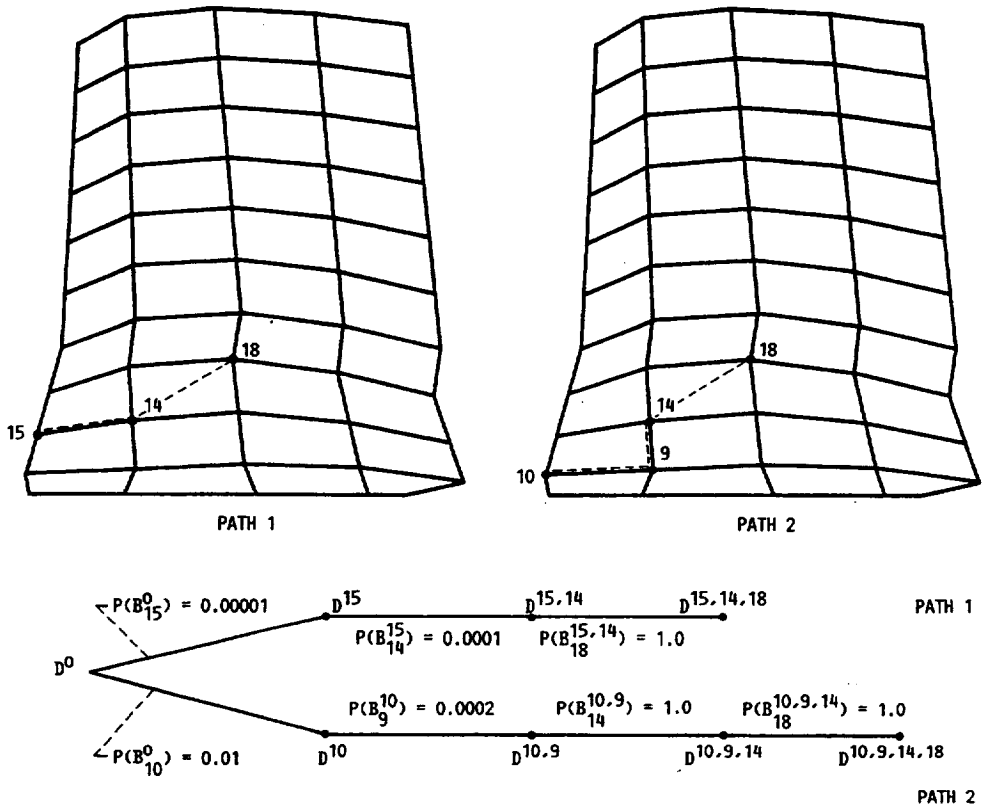

FIGURE 18. - MOST PROBABLE DAMAGE PATH CAUSED BY 100 000 CYCLES, WHERE D INDICATES DAMAGE STATES AT VARIOUS NODES AND P(B) INDICATES THE PROBABILITY THAT THE NEXT DAMAGE EVENT WILL OCCUR AT A PARTICULAR NODE.

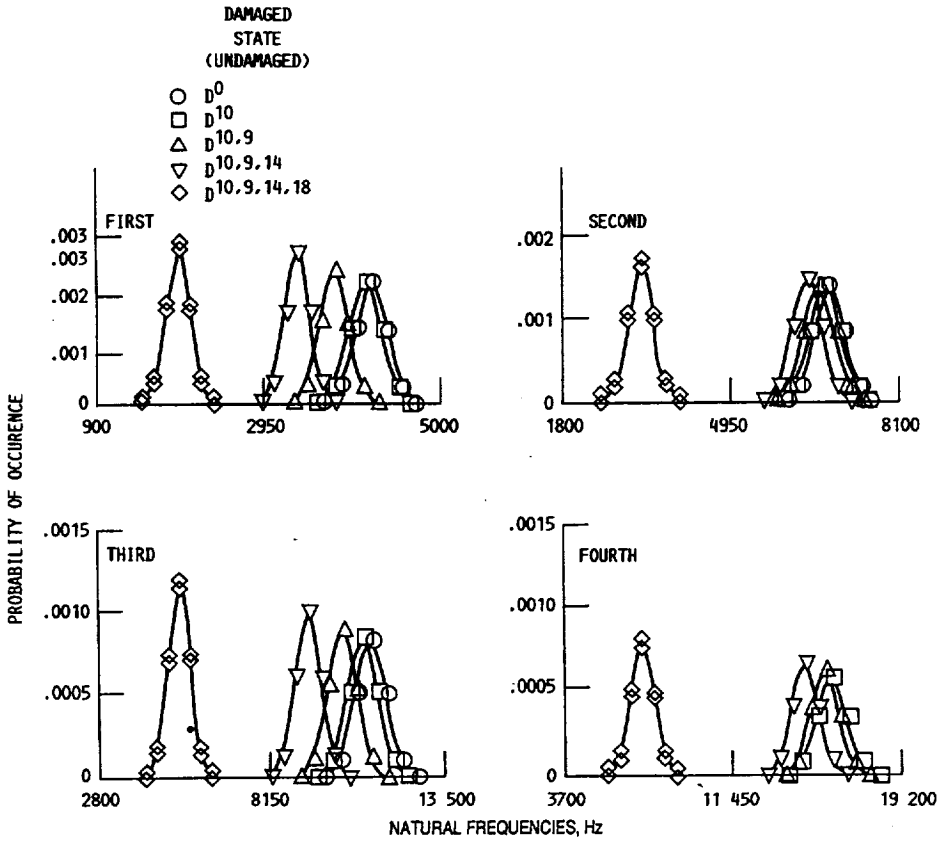

FIGURE 19. - CHANGE OF NATURAL FREQUENCIES IN DAMAGE PATH 2.

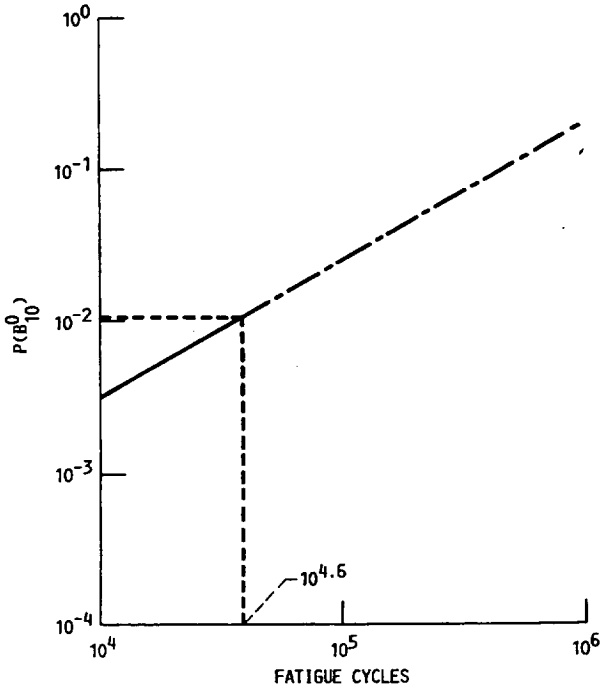

FIGURE 20. - PROBABILITY OF CRACK INITIATION AT NODE 10 AT DAMAGED STATE D^0 (OR $P(B^0_{10})$).

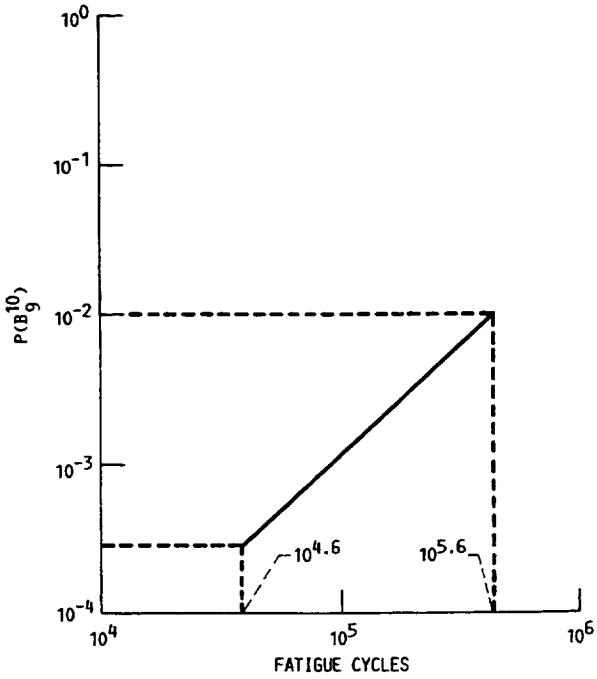

FIGURE 21.—PROBABILITY OF CRACK BEING EXTENDED TO NODE 9 AT DAMAGED STATE D^{10} (OR $P(B^{10}_9)$).

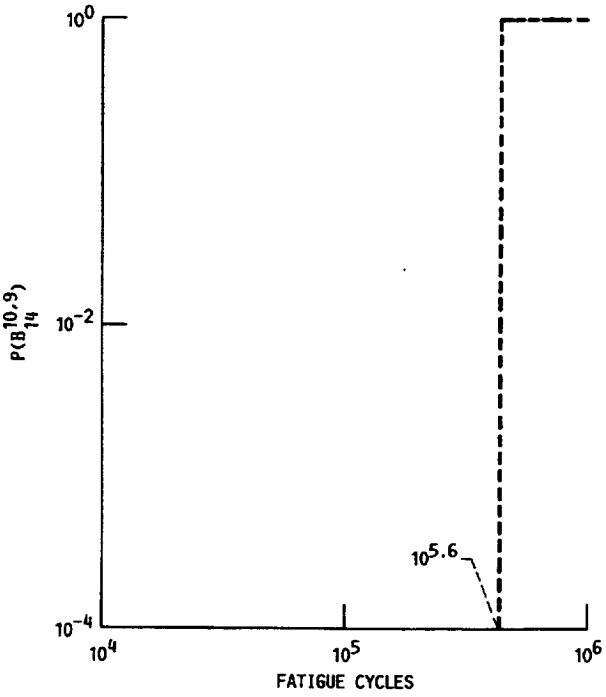

FIGURE 22.—PROBABILITY OF CRACK BEING EXTENDED TO NODE 14 AT DAMAGED STATE $D^{10,9}$ (OR $P(B_{14}^{10,9})$).

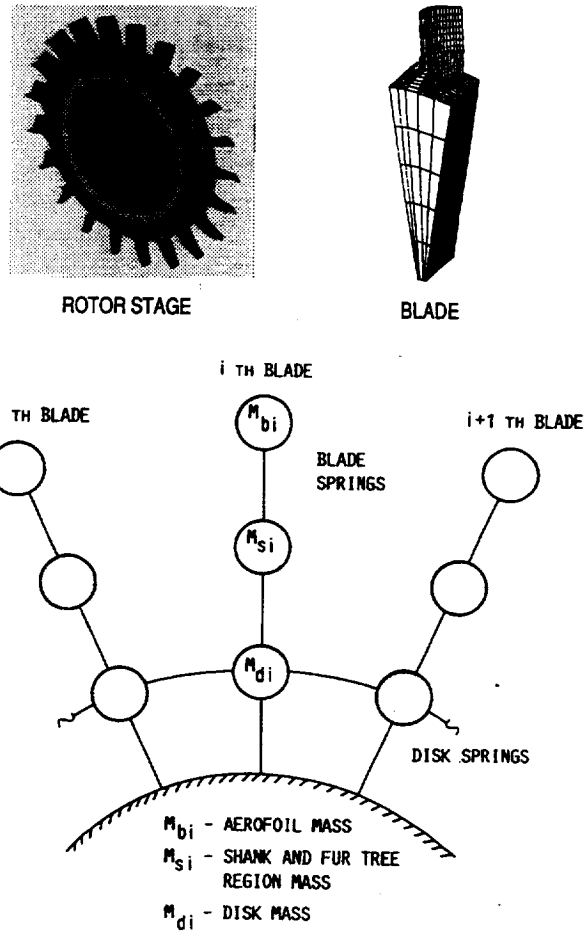

FIGURE 23.—LUMPED MASS-SPRING MODEL FOR BLADED DISK.

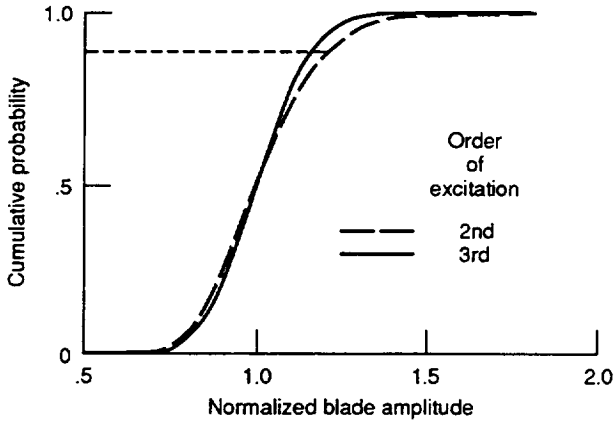

FIGURE 24.—CDF OF NORMALIZED BLADE AMPLITUDE (ROTOR WITH 10 BLADES).

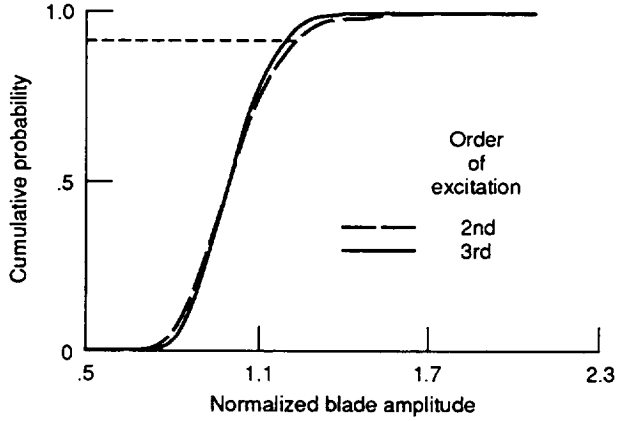

FIGURE 25.—CDF OF NORMALIZED BLADE AMPLITUDE (ROTOR WITH 20 BLADES).

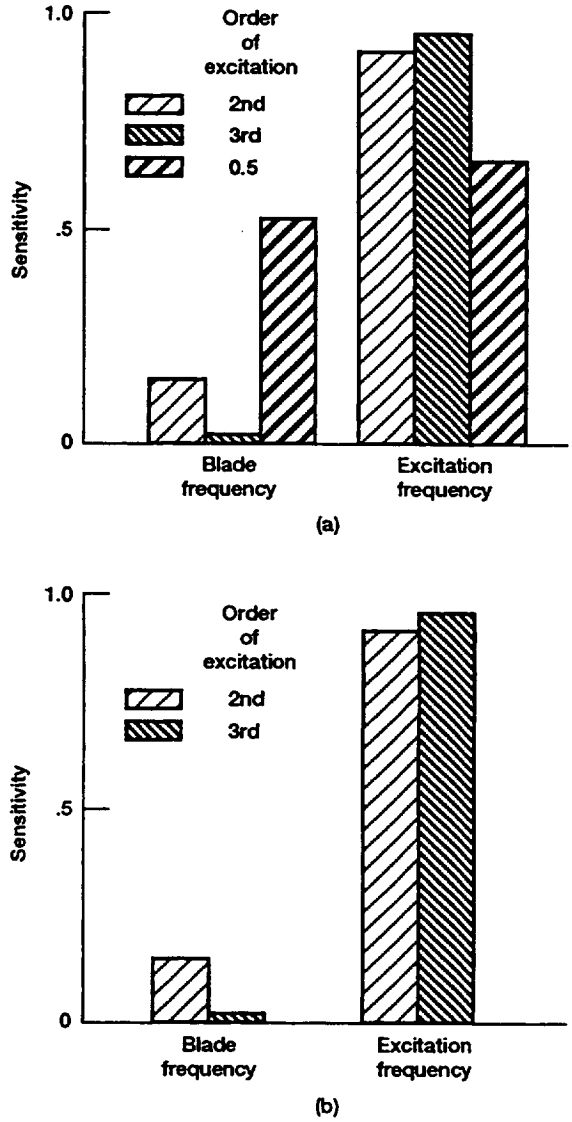

(a) Rotor with 10 blades.
(b) Rotor with 20 blades.

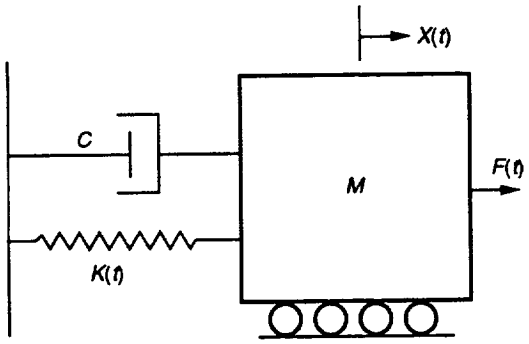

FIGURE 27.—SINGLE-DEGREE-OF-FREEEDOM OSCILLATOR SUBJECTED TO RANDOM EXCITATION.

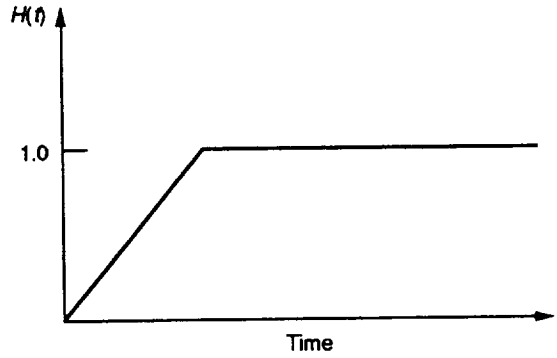

FIGURE 28.—MODULATING FUNCTION $H(t)$.

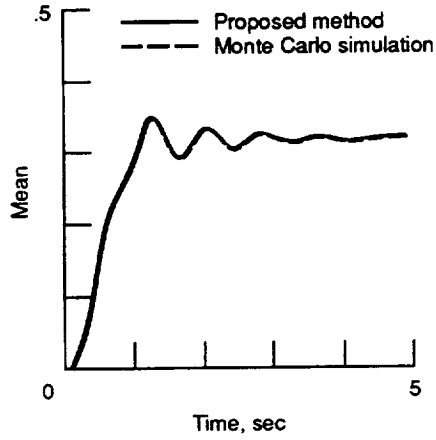

(a) MEAN.

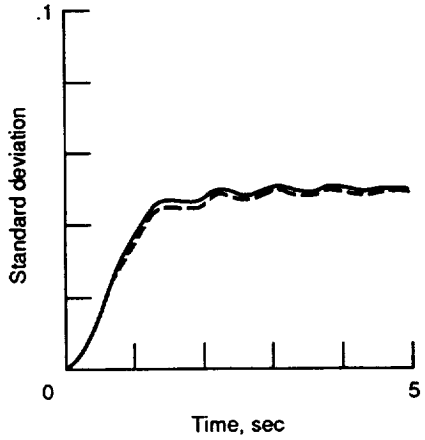

(b) STANDARD DEVIATION.

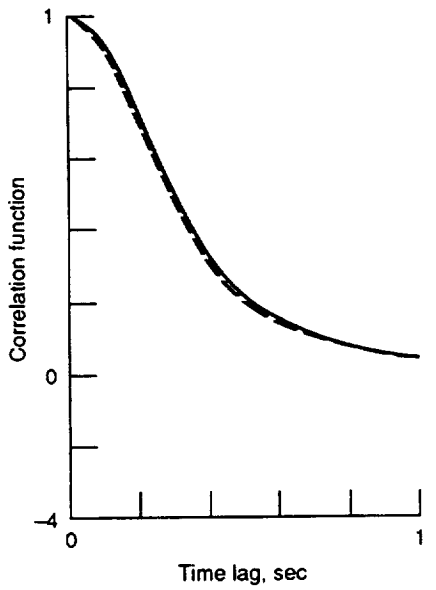

(c) AUTOCORRELATION FUNCTION AT 1 sec.

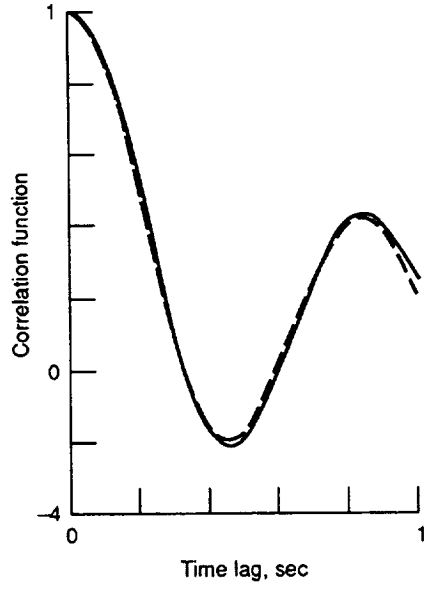

(d) AUTOCORRELATION FUNCTION AT 5 sec.

FIGURE 29.—STATISTICS OF DISPLACEMENT IN EQUATION (19) (C_S IN EQUATION (22) = 5).

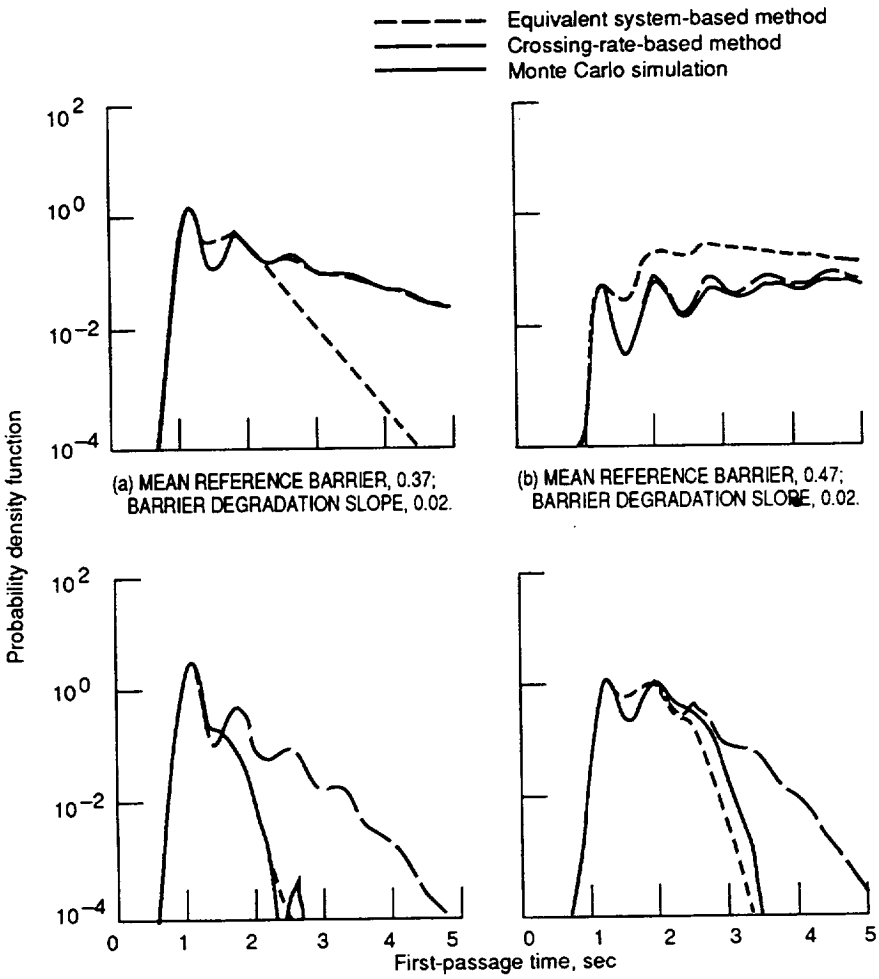

FIGURE 30.—PROBABILITY DENSITY FUNCTION OF FIRST-PASSAGE TIME (C_S IN EQ. (22) = 5; COEFFICIENT OF VARIATION OF REFERENCE BARRIER, 0, TYPE A DETERMINISTIC BARRIER MODEL).

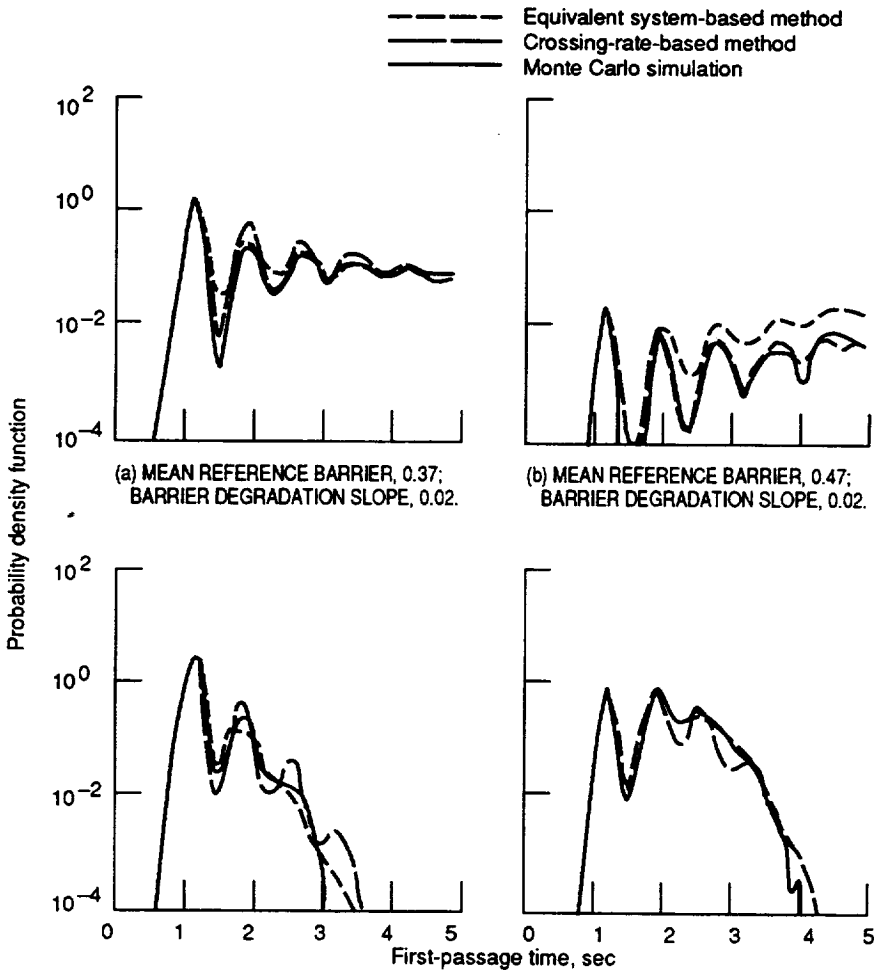

FIGURE 31.—PROBABILITY DENSITY FUNCTION OF FIRST-PASSAGE TIME (C_s IN EQ. (22) = 1; COEFFICIENT OF VARIATION OF REFERENCE BARRIER, 0, TYPE A DETERMINISTIC BARRIER MODEL).

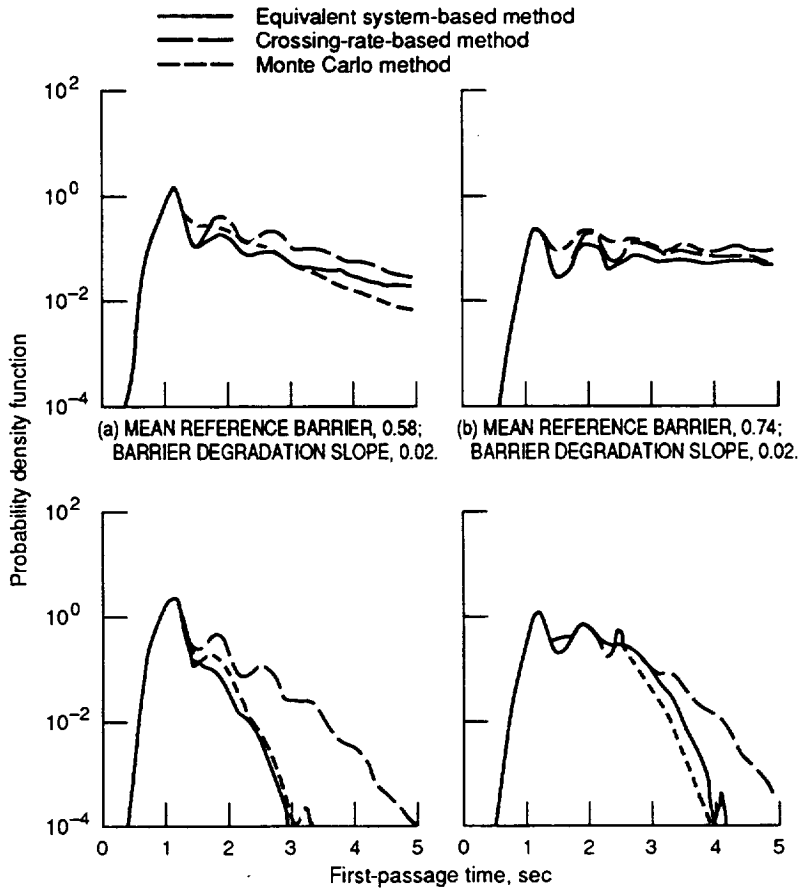

(a) MEAN REFERENCE BARRIER, 0.58; BARRIER DEGRADATION SLOPE, 0.02.

(b) MEAN REFERENCE BARRIER, 0.74; BARRIER DEGRADATION SLOPE, 0.02.

(c) MEAN REFERENCE BARRIER, 0.58; BARRIER DEGRADATION SLOPE, 0.15.

(d) MEAN REFERENCE BARRIER, 0.74; BARRIER DEGRADATION SLOPE, 0.15.

FIGURE 32.—PROBABILITY DENSITY FUNCTION OF FIRST-PASSAGE TIME (C_S IN EQ. (22) = 5; COEFFICIENT OF VARIATION OF REFERENCE BARRIER, 0.1; TYPE B RANDOM BARRIER MODEL).

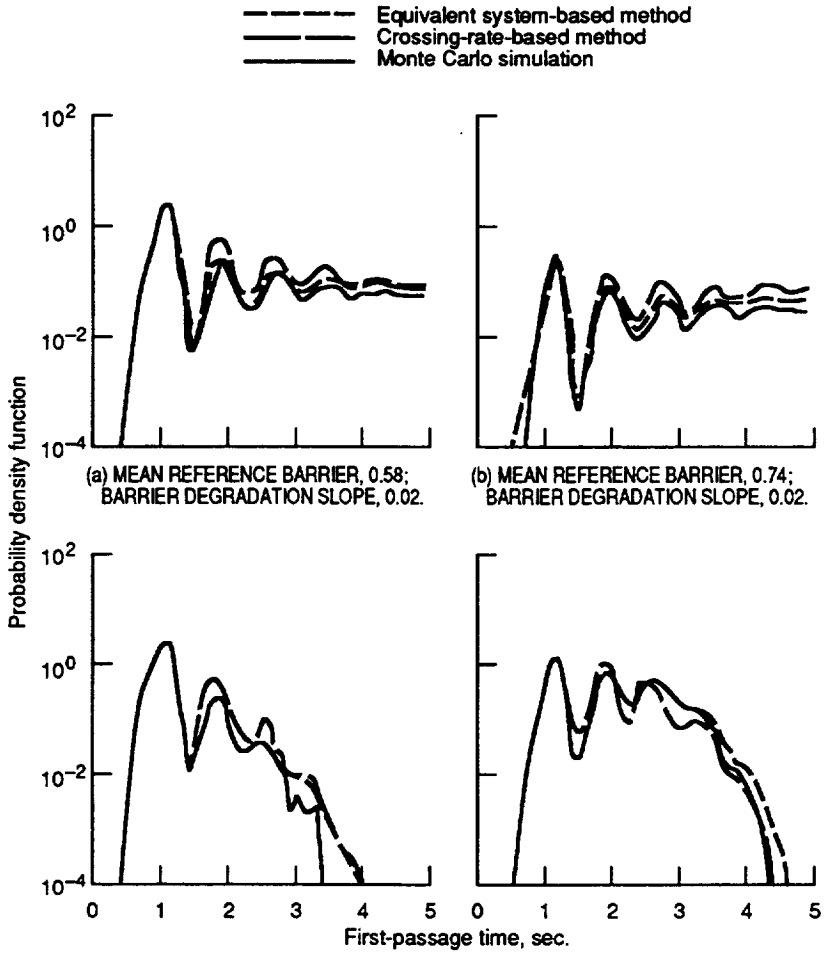

(a) MEAN REFERENCE BARRIER, 0.58; BARRIER DEGRADATION SLOPE, 0.02.

(b) MEAN REFERENCE BARRIER, 0.74; BARRIER DEGRADATION SLOPE, 0.02.

(c) MEAN REFERENCE BARRIER, 0.58; BARRIER DEGRADATION SLOPE, 0.15.

(d) MEAN REFERENCE BARRIER, 0.74; BARRIER DEGRADATION SLOPE, 0.15.

FIGURE 33.—PROBABILITY DENSITY FUNCTION OF FIRST-PASSAGE TIME (C_s IN EQ. (22) = 1; COEFFICIENT OF VARIATION OF REFERENCE BARRIER 0.1; TYPE B RANDOM BARRIER MODEL).

REPORT DOCUMENTATION PAGE

Form Approved
OMB No. 0704-0188

1. AGENCY USE ONLY (*Leave blank*)	2. REPORT DATE	3. REPORT TYPE AND DATES COVERED
	March 1992	Technical Memorandum

4. TITLE AND SUBTITLE

Probabilistic Evaluation of Uncertainties and Risks in Aerospace Components

5. FUNDING NUMBERS

WU-505-63-53

6. AUTHOR(S)

A.R. Shah, M.C. Shiao, V.K. Nagpal, and C.C. Chamis

7. PERFORMING ORGANIZATION NAME(S) AND ADDRESS(ES)

National Aeronautics and Space Administration
Lewis Research Center
Cleveland, Ohio 44135-3191

8. PERFORMING ORGANIZATION REPORT NUMBER

E-6240

9. SPONSORING/MONITORING AGENCY NAME(S) AND ADDRESS(ES)

National Aeronautics and Space Administration
Washington, D.C. 20546-0001

10. SPONSORING/MONITORING AGENCY REPORT NUMBER

NASA TM-105603

11. SUPPLEMENTARY NOTES

Invited chapter for Computational Nonlinear Mechanics in Aerospace Engineering, Progress in Astronautics and Aeronautics, edited by Satya N. Atluri. A.R. Shah, M.C. Shiao, and V.K. Nagpal, Sverdrup Technology, Inc., Lewis Research Center Group, 2001 Aerospace Parkway, Brook Park, Ohio 44142; C.C. Chamis, NASA Lewis Research Center. Responsible person, C.C. Chamis, (216) 433-3252.

12a. DISTRIBUTION/AVAILABILITY STATEMENT

Unclassified - Unlimited
Subject Category 39

12b. DISTRIBUTION CODE

13. ABSTRACT (*Maximum 200 words*)

This paper summarizes a methodology developed at NASA Lewis Research Center which computationally simulates the structural, material, and load uncertainties associated with Space Shuttle Main Engine (SSME) components. The methodology has been applied to evaluate the scatter in static, buckling, dynamic, fatigue, and damage behavior of the SSME turbo pump blade. Also calculated are the probability densities of typical critical blade responses, such as effective stress, natural frequency, damage initiation, most probable damage path, etc. Risk assessments have been performed for different failure modes, and the effect of material degradation on the fatigue and damage behaviors of a blade have been calculated using a multi-factor interaction equation. Failure probabilities for different fatigue cycles have been computed and the uncertainties associated with damage initiation and damage propagation due to different load cycle have been quantified. Evaluations on the effects of mistuned blades on a rotor have been made; uncertainties in the excitation frequency have been found to significantly amplify the blade responses of a mistuned rotor. The effects of the number of blades on a rotor have been studied. The autocorrelation function of displacements and the probability density function of the first passage time for deterministic and random barriers for structures subjected to random processes also have been computed. A brief discussion has been included on the future direction of probabilistic structural analysis.

14. SUBJECT TERMS

Uncertainties; Probability density function; Cumulative distribution function; Factorial design; Monte-Carlo; Probability of failure; Sensitivity; Degradation; Damage initiation; Damage propagation; Fatigue; Mistuning; Random process; Stationary; Nonstationary; Autocorrelation; Crossing rate; First passage

15. NUMBER OF PAGES

48

16. PRICE CODE

A03

17. SECURITY CLASSIFICATION OF REPORT	18. SECURITY CLASSIFICATION OF THIS PAGE	19. SECURITY CLASSIFICATION OF ABSTRACT	20. LIMITATION OF ABSTRACT
Unclassified	Unclassified	Unclassified	